Sustainable Energy & Fuels

ROYAL SOCIETY OF CHEMISTRY

REVIEW

View Article Online
View Journal | View Issue

Cite this: *Sustainable Energy Fuels*, 2024, **8**, 1588

Multinuclear systems for photo-induced production of green fuels: an overview of homogeneous catalysts based on transition metals

Alessandro Amadeo,†[ab] Emanuele La Mazza,†[a] Antonino Arrigo,[a] Giuseppina La Ganga[a] and Ambra M. Cancelliere *[a]

Received 15th January 2024
Accepted 13th March 2024

DOI: 10.1039/d4se00078a

rsc.li/sustainable-energy

In the last century, humankind has based its energy demand on the extensive exploitation of fossil resources with the massive emission of CO_2, resulting in problems such as pollution, the greenhouse effect, and, consequently, climate change. However, these resources are limited, and each year, their depletion is getting closer. Therefore, in the last few decades, scientific efforts have been focused on finding alternative ways to use and store green energy sources. The purpose of the present review is to present an overview of the most efficient multinuclear catalytic systems in the field of artificial photosynthesis based on reductive and oxidative mechanisms. In particular, it emphasizes the most recent improvements in homogeneous photocatalysis based on multimetallic complexes, illustrating the advantages of systems consisting of a linked catalyst(s) and photosensitizer(s) that can be employed to achieve high-energy demanding processes, such as the reduction of CO_2 and water oxidation.

1. Introduction

As the earth's population grows and time progresses, the energy demand cannot be ignored. Since the Industrial Revolution, the welfare of society has been based on carbon, and later fossil fuels, with a gradually increasing awareness that this regime of non-renewable sources cannot sustain both human beings and the planet in the long term. There are two problems related to our current lifestyle: (i) the prolonged and excessive exploitation of finite fossil fuel reservoirs will inevitably lead to their exhaustion, with a significant overall economic impact due to the continuous increase in the cost of producing and purchasing them[1–3] and (ii) the combustion process to obtain energy from fossil fuels involves increasing the concentration of greenhouse gases, such as CO_2, in the atmosphere,[4] as well as the production of smog, which is harmful to human health (and other living organisms).

Accordingly, in the last few decades, efforts have been devoted to making the global energy demand independent of exhaustible and environmentally toxic fuels. Among the potential solutions, the use of clean and renewable energy sources[5] such as solar energy has been found to be one of the most promising options. In this case, nowadays, research is focused on the energy-efficient production of H_2,[6–8] CO, formic acid[9–12] and other solar fuels/energy carriers through reactions promoted by visible light. Ideally, the simplest ways to achieve this involve photoinduced water splitting to obtain H_2 (reduction process) and O_2 (oxidation process)[13] and the photoinduced reduction of CO_2 into CO and/or formic acid. However, all these reactions are characterized by two common factors: they are associated with reactants that do not absorb visible light and involve multi-electron processes. Thus, it is not possible to realize these processes by simple irradiation. Well-designed photosensitizers require species that may absorb visible light to promote electron-transfer processes and catalysts, *i.e.* species that may accumulate electrons or holes to achieve the overall redox reaction.[14] In this regard, mainly semiconductors (for heterogeneous catalysis) and transition metal complexes (for homogeneous catalysis) have been developed as catalytic systems through several methods such as photocatalysis, electrochemistry and photo-electrochemistry.

This review focuses on the photocatalytic processes to obtain water oxidation and CO_2 reduction using multinuclear catalysts in a homogeneous phase. Fundamentally, transition metals are in the spotlight of this research field because they are characterized by various oxidation states, which combine perfectly with the requirement to achieve multi-electron processes;[15] in fact, the photoexcitation of a molecule typically leads to a single oxidized or reduced species because the excitation with a single photon can only trigger a one-electron transfer process. Therefore, to achieve a multi-electron reaction, cyclic processes are required, where for every photon absorbed, a charge (positive or negative) is accumulated on the catalyst, eventually leading to

[a]*Dipartimento di Scienze Chimiche, Biologiche, Farmaceutiche e Ambientali, Interuniversitary Research Center on Artificial Photosynthesis (SOLAR-CHEM, Messina node), University of Messina, Via F. Stagno d'Alcontres 31, 98166 Messina, Italy. E-mail: acancelliere@unime.it*

[b]*2DCBB, University of Perugia, Via dell'Elce di sotto, 8, 06123, Perugia, Italy*

† These authors contributed equally to this work.

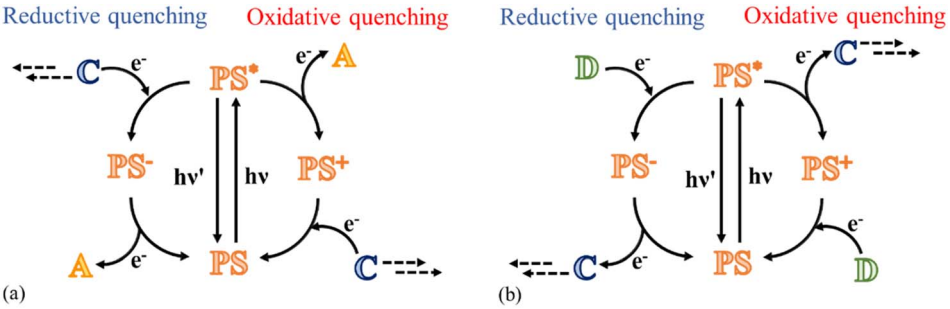

Fig. 1 Schematic of photoinduced catalysis for (a) water oxidation and (b) CO_2 reduction processes. Reductive and oxidative quenching mechanisms are illustrated (on the left and right side, respectively). **A** is the electron-acceptor species, **D** is the electron-donor species, **PS** is the photosensitizer and **C** represents the catalyst.

a species capable of participating in reactions with high-energy requirements (Fig. 1a and b).

In addition to the photosensitizer and catalyst, to complete the catalytic cycle, a species that acts as an electron donor or acceptor is necessary, depending on the cycle considered, enabling the excited photosensitizer to be reduced or oxidized. Ideally, an optimal sacrificial agent would be the solvent itself, but the Gibbs energy for this type of reaction is generally too high,[18] and thus other compounds dissolved in solution are usually used, for example, sodium persulfate or pentaamminechlorocobalt(III)chloride for the oxidative side and BIH (1,3-dimethyl-2-phenylbenzimidazoline) and BNAH (1-benzyl-1,4-dihydronicotinamide) for the reduction processes.[16]

Multinuclear complexes are species in which two or more metals are connected to each other through bridging ligands.[17] If a metal complex catalyst is used, this species may be considered a "supramolecular catalyst". Supramolecular photocatalysis offers the benefit of fast electron transfer processes between the components, given that diffusion and collision components between subunits are not required, thereby enhancing the overall performance of the photocatalytic system.[18–20] Consequently, this results in increased durability of the photosensitizer subunits. In fact, the more rapidly consumed excited and/or reduced state leads to the acceleration of the photocatalytic reaction.[21]

Based on all these reasons, the aim of this review is to focus attention on the advantage of connecting two or more catalytic subunits to increase the photocatalytic performances of an artificial photosynthetic supramolecular system. Thus, we explore the development in the last decade of the water oxidation part of the system (the actual bottleneck of the entire process), and regarding the reducing part, we will investigate only the processes for CO_2 reduction, given that the water reduction to H_2 is widely discussed.[22]

2. Multinuclear species in water oxidation reaction

The bottleneck of all photosynthetic processes is the half-reaction of water oxidation to O_2 molecules. The overall water splitting reaction is represented by eqn (1):

$$H_2O\ (l) \rightarrow \tfrac{1}{2}\,O_2\ (g) + H_2\ (g) \quad (1)$$

which may be expressed through the following half-reaction equations:

$$2H^+ + 2e^- \rightarrow H_2 \quad E^\circ = 0\ V\ vs.\ SHE \quad (2)$$

$$2H_2O \rightarrow O_2 + 4H^+ + 4e^- \quad E^\circ = 1.23\ V\ vs.\ SHE \quad (3)$$

In the last few decades, numerous reports have been published on the light-driven production of hydrogen from water,[23] and nowadays efforts in this regard are focused on optimizing the process rather than implementing it.

Alternatively, more efforts are required to achieve oxygen evolution from water, given that it requires the formation of an O–O bond, and simultaneously the transfer of 4 electrons and $4H^+$; consequently, this leads to substantial energy barriers and slow kinetics, making the overall process more challenging to overcome them.[24,25] The result is the potential needed to achieve oxygen evolution being greatly affected by the high overpotential, thus requiring a more positive potential than 1.23 V *vs.* SHE. This potential should be quite high to access using energy provided by light. Therefore, significant effort has been devoted to the realization of catalysts that can facilitate this reaction.

The catalytic oxidation mechanism of water involves several steps (Fig. 2), which can be grouped in three stages, as follows: (i) the formation of a highly-reactive metal-oxo species; (ii) the formation of O–O bonds; and (iii) O_2 evolution and catalyst restoration. In the first stage, a single water molecule is bound to the metal center of the catalytic subunit and successively activated in the form of an M=O species. The second stage is crucial, and generally may follow one of two possible paths, *i.e.*, water nucleophilic attack (WNA) and interaction of two M=O units (I2M). In the WNA mechanism, a molecule of water acts as the nucleophilic agent, targeting the electrophilic metal-oxo sites, generating a hydroperoxide species. Instead, in the I2M mechanism, the radical coupling of two metal-oxo sites occurs, leading to their dimerization and generation of an M–O–O–M species. In the case of both mechanisms, the latter step is the oxidation of the intermediate and the evolution of O_2.[26–29]

In the last few decades, research was centered on developing water oxidation catalysts (WOCs) based on metal oxide

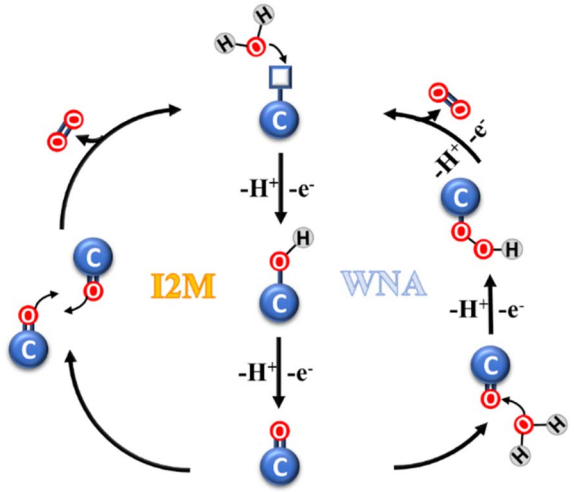

Fig. 2 Schematic representation of the two mechanisms of catalytic water oxidation.

materials or molecular transition-metal (Ru, Fe, Mn, Co, Ir, *etc.*) complexes to improve the selectivity, efficiency and stability of the system.[30]

Although several examples of first-row transition-metal WOCs have been reported recently, ruthenium complexes are still the most studied systems due to their long-lived ^{3}MLCT state, redox stability and high absorption in the UV-vis spectrum.[31] In 2009, Sun and group developed an interesting complex, [Ru(bda)(pic)$_2$] (bda = 2,2′-bipyridine-6,6′-dicarboxylate, pic = picoline)[32] (see Fig. 3), which showed outstanding efficiency such as TON = 2000 and TOF = 41 s^{-1}, using cerium(IV) ammonium nitrate (CAN) as the oxidizing agent at pH 1.

Since then, numerous new systems based on [Ru(bda)(pic)$_2$] have been studied, trying to achieve better efficiency. Looking to nature (the multimetallic Mn_4CaO_5 oxygen evolving center) and to the first reported catalysts, such as the so-called "blu dimer"[33] and others,[34] an interesting approach involving the assembly of multinuclear structures,

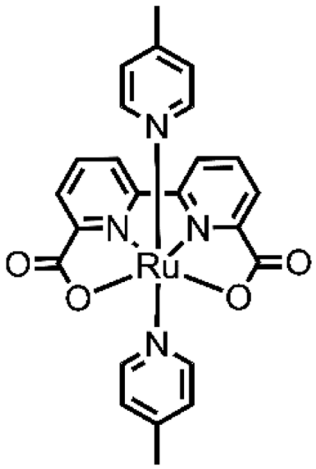

Fig. 3 Chemical structure of the [Ru(bda)(pic)$_2$] catalyst.

which include multiple catalytic centers. The positive aspects of type kind of design are the increased stability of the catalytic units, which are now bound together (thus the decomposition of the ligand, one of the most common deactivation pathways of catalysts, is more difficult). Others positive aspects are the increased efficiency due to the electronic communication between the components of the system and the possibility to modulate the shape of this structure and the way they interact each other and with other subunits in the system. Moreover, a multinuclear catalyst sometimes can use a different mechanism from the mononuclear one. This is the case of [Ru(bda)(pic)$_2$], which when free in solution, oxidizes water through an I2M mechanism, and in multinuclear complexes, the mechanism reaction can shift to WNA. The catalytic and photocatalytic performances (with the respective experimental conditions) of all the catalyst metal complexes for the oxygen evolution reported in this review are summarized in Table 1. The comparison with the homologue monomeric species is reported in the main text.

2.1 Multinuclear catalysts based on Ru(bda) moieties

An interesting example of a system that connects two or more catalytic subunits with a suitable bridging ligand can be found in the report published by Sun in 2016. Briefly, Sun compared the efficiencies of di- and trinuclear catalysts based on Ru(bda) units linked by bis- or tris(pyridylethyl)benzene[35] (**1** and **2** in Fig. 4, respectively).

These systems have been tested for both the chemical and photochemical water oxidation. In the first case, CAN was used as the chemical oxidant agent in aqueous solution at pH 1 for triflic acid. Good performances were recorded for both systems, where dinuclear catalyst (**1**) exhibited a turnover number (TON) of 22 206 and turnover frequency (TOF) of 34 s^{-1} per Ru center, while the trinuclear catalyst (**2**) exhibited a TON of 28 832 and TOF of 42 s^{-1} per Ru unit. Each catalytic unit of these multinuclear complex catalysts shows better performances than the mononuclear catalyst used as the reference (TON of 1460 and TOF of 3.8 s^{-1}). This can be explained by hypothesizing the advantageous cooperation between two metal centers. To collect more information about the catalytic mechanism, kinetic studies have been carried out to monitor the CAN consumption with UV-vis spectrometry. The results obtained by these experiments confirmed a first-order reaction for each the binuclear and trinuclear systems, even if it is not clear whether the pathway is I2M between two metal centers linked together or WNA type. These multinuclear systems have also been tested for light-driven water oxidation using [Ru(bpy)$_2$(4,4′-EtOOC$_2$-bpy)](PF$_6$)$_2$ as the photosensitizer and $Na_2S_2O_8$ as the sacrificial oxidant. The binuclear catalyst showed a TON of 369, while that of the trinuclear catalyst was 535.

A new way to build multinuclear catalysts consists of assembling many catalytic units in a polymeric arrangement, which are more stable and often easier to produce than mononuclear catalysts. In this frame, Würthner designed, synthesized and studied new oligomeric chains based on Ru(bda), in which the metal centers are linked by 1,4-di(pyridin-

Table 1 Catalytic and photocatalytic performances of the reported complexes for water oxidation

	Chemical catalysis			Photocatalysis			
Catalyst	TON	TOF	Experimental conditions	TON	TOF	Φ	Experimental conditions
1	22 206	34 s^{-1}	CAN, pH 1 for triflic acid	369			PS: $[Ru(bpy)_2(4,4'\text{-}EtCOO_2\text{-}bpy)](PF)_6$ SA: $Na_2S_2O_8$[a]
2	28 832	42 s^{-1}	CAN, pH 1 for triflic acid	535			
3	—	—		>1000[b]	14 s^{-1}		PS: $[Ru(deeb)_2(bpy)]Cl_2$ SA: $Na_2S_2O_8$ Phosphate buffer (pH 7.2) and CH_3CN as co-solvent
4	7400[b]	155 s^{-1} [b]		1255	13.1 s^{-1}		PS: $[Ru(bpy)_3]Cl_2$ SA: $Na_2S_2O_8$ Phosphate buffer (pH 7.2) and CH_3CN (1 : 1, v/v)
5	5200	147 s^{-1}	CAN, pH 1 (CH_3CN 30%)				
6	2200	72 s^{-1}	CAN, pH 1 for triflic acid				
7	—	12 s^{-1}	CAN, pH 1 for triflic acid (CH_3CN 50%)	36	1.1 s^{-1}		PS: $[Ru(bpy)_3]Cl_2$ SA: $Na_2S_2O_8$ Phosphate buffer (pH 7) and CH_3CN (1 : 1, v/v)
8	—	26 s^{-1}	CAN, pH 1 for triflic acid (CH_3CN 50%)	400	10 s^{-1}		PS: $[Ru(bpy)_3]Cl_2$ SA: $Na_2S_2O_8$ Phosphate buffer (pH 7) and CH_3CN (1 : 1, v/v)
9	—	42 s^{-1}	CAN, pH 1 for triflic acid (CH_3CN 50%)	500	23 s^{-1}		PS: $[Ru(bpy)_3]Cl_2$ SA: $Na_2S_2O_8$ Phosphate buffer (pH 7) and CH_3CN (1 : 1, v/v)
10				460	15.5 s^{-1}		PS: $[Ru(bpy)_3]Cl_2$ SA: $Na_2S_2O_8$ Phosphate buffer (pH 7) and CH_3CN (40%)
11	56	0.8 s^{-1}	$[Ru(bpy)_3](ClO_4)_3$, pH 8	150			PS: $[Ru(bpy)_3](ClO_4)_2$ SA: $Na_2S_2O_8$
Ru_4POM						0.3	PS: $[Ru\{(\mu\text{-}dpp)Ru(bpy)_2\}_3](PF_6)_8$ SA: $Na_2S_2O_8$ Phosphate buffer (pH 7)
$[Co_4(H_2O)_2(PW_9O_{34})_2]^{10-}$						0.34	PS: $[Ru(bpy)_3]Cl_2$ SA: $Na_2S_2O_8$
$[Mn_3(H_2O)_3(SbW_9O_{33})_{12}]^{12-}$				103		0.13	PS: $[Ru(bpy)_3]Cl_2$ SA: $Na_2S_2O_8$ Sodium borate buffer (pH 9)
$[(V^{IV}5V^{V})O_7(OCH_3)_{12}]^-$						0.2	PS: $[Ru(bpy)_3]Cl_2$ SA: $Na_2S_2O_8$ Phosphate buffer (pH 7)
12				178	3.6 s^{-1}	0.38	PS: $[Ru(bpy)_3](ClO_4)_2$ SA: $Na_2S_2O_8$ Sodium borate buffer (pH 9)
13					0.4 min^{-1}		SA: $Na_2S_2O_8$ $NaHCO_3$ buffer (pH 7)
14					1.4 min^{-1}		SA: $Na_2S_2O_8$ $NaHCO_3$ buffer (pH 7)

[a] PS refers to photosensitizer species and SA is the sacrificial agent used in the photocatalytic cycle. [b] The reference, $[Ru(bda)(pic)_2]$, under the same experimental conditions showed a TON of 970 and TOF of 8.4 s^{-1}.

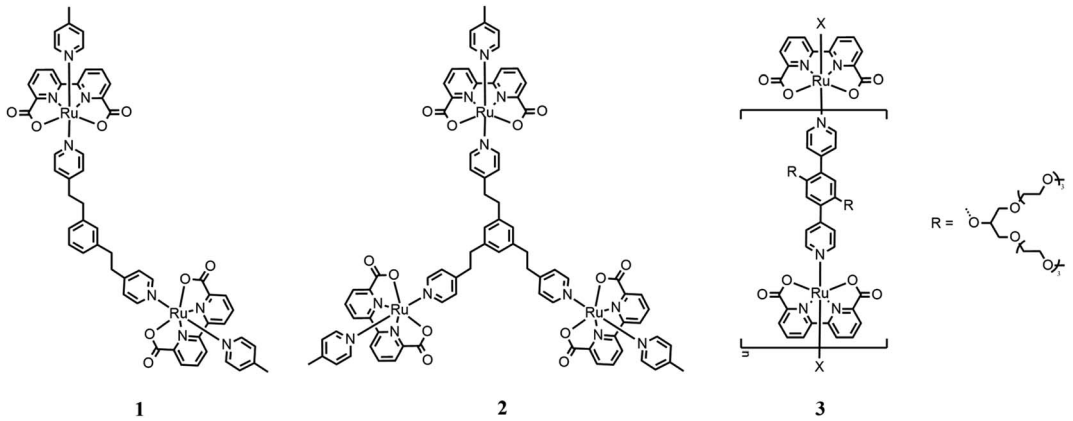

Fig. 4 Chemical structures of dinuclear (**1**) and trinuclear (**2**) catalysts. Catalyst **3** represents oligomeric species.

4-yl)benzene substituted with oligoethylene glycol groups to enhance the solubility of the oligomeric species (**3** in Fig. 4).[36]

By tuning the synthetic conditions, researchers have been able to build three different categories of species, which differ by the length of their chain. It is difficult to precisely determine the number of units in the chains because different characterization techniques presented contrasting results due to the different methods used to collect the data. These species have been tested for photocatalytic water oxidation using $[Ru(deeb)_2(bpy)]Cl_2$ (deeb = diethyl 2,2′-bipyridine-4,4′dicarboxylate, bpy = 2,2′-bipyridine) as the photosensitizer and $Na_2S_2O_8$ as the sacrificial oxidant in an aqueous solution of phosphate buffer (pH 7.2) and CH_3CN as the co-solvent in various ratio. It has been observed that the performances of all three categories of compounds improved with a decrease in the concentration of CH_3CN. Moreover, the efficiency of the oligomers increased with chain length, resulting in a TOF of ~14 s^{-1} and TON of >1000 for the larger categories of compounds in pure water. Under the same conditions, the smallest compounds showed a lower efficiency with the TOF of 9.5 s^{-1} and TON of 640. Kinetic investigations were conducted and the results indicated an I2M pathway due to the intra-assembly aggregation of oligomeric fibers, especially with a low amount of CH_3CN or in pure water. These materials are very promising due to their high stability and simplicity of their synthesis due to the self-assembly mechanism.

2.1.1 Macrocyclic systems based on Ru(bda) moieties. In recent years, another interesting approach that has been used to improve the performances of $[Ru(bda)(pic)_2]$ involves incorporating it in a supramolecular macrocycle. In 2016, Würthner reported the preparation and study of $[Ru(bda)bpb]_3$ (bpb = 1,4-bis(pyrid-3-yl)benzene),[37] a trinuclear macrocycle (**4** in Fig. 5).

This macrocycle was tested as catalyst for water oxidation using CAN as the chemical oxidant in aqueous solution at pH 1. The best performance was achieved using 59% of CH_3CN, which is necessary to allow good solubilization. Under these conditions, the efficiency gave a TON of 7400 (~2500 per Ru unit) and TOF of 155 s^{-1}. These values were compared to that one resulting from the same experiment using the mononuclear $[Ru(bda)(pic)_2]$ as a reference, which showed a TON of 970 and TOF of 8.4 s^{-1}, indicating that in the macrocyclic structure, the Ru(bda) units have enhanced activity and increased stability

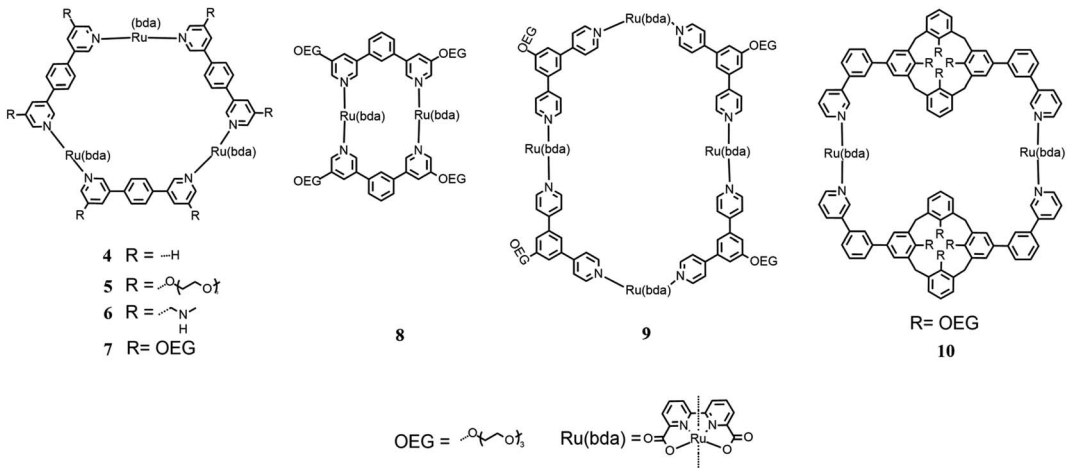

Fig. 5 Chemical structures of different macrocyclic catalysts.

due to the scaffold of the ring. Computational studies displayed the presence of up to ten water molecules preorganized inside the cavity, and this supramolecular effect probably contributes to the improved efficiency of each catalytic unit. These computational studies together with the kinetic studies showed that the mechanistic pathway followed by this macrocycle is WNA instead of I2M. This macrocycle was also tested for photocatalytic water oxidation jointly with $[Ru(bpy)_3]^{2+}$ as the photosensitizer and $Na_2S_2O_8$ as the sacrificial oxidant in a 1 : 1 acetonitrile/phosphate buffer (pH 7.2). This system appeared to also be efficient when diluted, *e.g.* with a concentration of the catalyst of 90 nM, showing a TON of ~1.255 and TOF of ~13.1 s^{-1}.

In 2017, Würthner modified this macrocycle substituting a $-CH_2NMe_2$ group and triethylene glycol in the meta position of all pyridines (**5** and **6** in Fig. 5)[38] to increase the solubility of the macrocycle in water and avoid the use of large amounts of CH_3CN as the cosolvent, which is one of the principal ways for the deactivation of the catalyst.

Chemical water oxidation with different CH_3CN/H_2O ratios was tested using CAN as the oxidant. In the case of the macrocycle substituted with triethylene glycol, the CH_3CN concentration could be reduced to 30%, obtaining a TOF of 147 ± 9 s^{-1} and TON of 5.2×10^3. The macrocycle with a $-CH_2NMe_2$ group was investigated in water without cosolvent (pH 1 for triflic acid) and a TON of 2.2×10^3 and TOF of 72 ± 6 s^{-1} were recorded.

In 2021, the photocatalytic performances for the water oxidation of the latter macrocycle were investigated and compared with $[Ru(bda)bpb]_3$ (**4** in Fig. 5) using different substituted $[Ru(bpy)_3]^{2+}$ as the photosensitizers,[39] as shown in Fig. 6.

In the same year, Würthner published a study on new macrocycles similar to $[Ru(bda)bpb]_3$ but containing two and four catalytic units each, $[Ru(bda)bpb]_2$ and $[Ru(bda)bpb]_4$ (**8** and **9** in Fig. 5), respectively.[40] Each linker between the catalytic units of these supramolecular systems was differently substituted in the ortho position with oligoethylene glycol groups to improve the solubility of the system in water. In this paper, the authors compared the catalytic activity of these systems for water oxidation, focusing on the dependence of the efficiency on the size of the ring. For the first time, the efficiency of these systems toward chemical water oxidation was tested using CAN as the sacrificial oxidant in a solution containing 50% of CH_3CN at pH 1 for triflic acid. The kinetic studies proved first-order kinetics according to the WNA mechanism. Macrocycles **7**, **8** and **9** in Fig. 5 (with two, three or four catalytic subunits) showed a TOF of 12 s^{-1}, 26 s^{-1}, and 42 s^{-1} (6 s^{-1}, 8.7 s^{-1}, and 10.5 s^{-1} per Ru unit), respectively. These results show that the performances increased with the size of the ring but not only because there are more catalytic units but also because each unit enhances the efficiency. The three systems were tested for photocatalytic water oxidation using $[Ru(bpy)_3]^{2+}$ as the photosensitizer and $Na_2S_2O_8$ as the sacrificial electron acceptor in a solution phosphate buffer/CH_3CN 1 : 1 at pH 7. The macrocycles with 2, 3 and 4 Ru(bda) units showed a TOF of 1.1 s^{-1}, 10 s^{-1}, and 23 s^{-1} (0.6 s^{-1}, 3.3 s^{-1}, and 5.8 s^{-1} per Ru) and TON of 36, 400, and 500 respectively. All these systems showed a higher TON per Ru unit than that of $[Ru(bda)(pic)_2]$ (under the same experimental conditions, the turnover number was 13), demonstrating the increased stability of the catalyst when it is organized in a supramolecular structure.

In the same year, Würthner tried a different approach for the realization of a new type of supramolecular catalyst using two calix[4] arenes, functionalized with oligoethylene glycol groups to enhance the total solubility of the system, and two Ru(bda) units using 2-phenilpyridine as linkers to realize a macrocycle (**10** in Fig. 5).[41]

Photocatalytic experiments were performed using $[Ru(bpy)_3]Cl_2$ as the photosensitizer and $Na_2S_2O_8$ as the sacrificial electron acceptor in phosphate buffer with 40% of CH_3CN at pH 7. These tests were performed at different concentrations of the catalyst in the range of 12–200 nM, and the TOF of 15.5 (7.5 per Ru unit) and TON of 460 were reported.

2.2 Catalyst with helicate structure

A global process for the conversion and storage of energy should involve abundant, easily available and economic materials to be

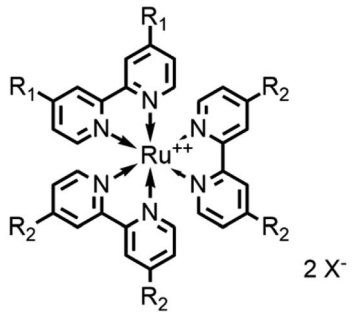

PS1: R_1 = H and R_2= H, X^-= Cl^-
PS2: R_1 = H and R_2= COOEt, X^-= PF_6^-
PS3: R_1 = COOH and R_2= COOH, X^-= Cl^-

Fig. 6 Different substituted photosensitizers.

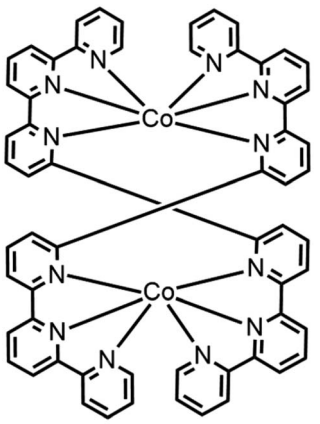

11

Fig. 7 Chemical structure of cobalt helicate $[Co_2(spy)_2](ClO_4)_4$.

sustainable from all points of view. In this perspective, recently, new catalysts have appeared in literature based on earth abundant transition metals, which represent a valid alternative for applications in future technologies, although they usually show lower performances than catalysts made of ruthenium.

One of the most studied elements for water oxidation is cobalt. It is now well established that CoO_x constitutes a good example of a water oxidation heterogeneous catalyst. Many Co complexes have been developed to act as homogeneous catalysts, but they usually act as just pre-catalysts because they are not active themselves but decompose into CoO_x. A very intriguing exception is represented by $[Co_2(spy)_2](ClO_4)_4$ (spy = 2,2′:6′,2″:6″,2‴:6‴,2⁗:6⁗,2⁗′-sexipyridine), a double-helical dicobalt(II), as shown in Fig. 7.[42]

$[Co_2(spy)_2]$ is constituted by two Co(II) units linked together by two spy ligands (each metal center is bound to a 2,2′:6′,2″-terpyridine fragment). This structure leads to a distorted octahedral geometry with an N–C–N angle of about 150°, unlike the ideal 180° that allows the coordination of a water molecule. This was tested as catalyst for water oxidation using $[Ru(bpy)_3](ClO_4)_3$ as the oxidant at pH 8, obtaining a TON of 56 and TOF of 0.8 s^{-1}. It has also been tested for light-driven water oxidation using $[Ru(bpy)_3](ClO_4)_2$ as the photosensitizer and $Na_2S_2O_8$ as the sacrificial agent, obtaining a TON of 150. These results are promising if we consider that analogous Co complexes such as $[Co(tpy)_2]^{2+}$ showed no activity under similar conditions. Further investigations were conducted to exclude that this molecule acts as a precatalyst and the results showed that more than 97% of oxygen was produced by the homogeneous catalyst and not by CoO_x.

2.3 Polyoxometalate (POM) catalysts

A new category of species that can be used as water oxidation catalysts is represented by polyoxometalates (POMs), which are completely inorganic species based on earth abundant elements. These structures are composed of a transition metal core linked to inorganic ligands. They show great solubility in water due to their high negative charge and high thermal and chemical stability due to the absence of organic moieties that usually oxidize or degrade.

The first paper dealing with POMs in oxygen evolving catalysis was reported in 2004[43] when Shannon *et al.*[43] observed electrochemical oxygen generation at low potentials (E_0 = 0.756 V *vs.* NHE), from a 2 μM aqueous solution of $Na_{14}[Ru_2Zn_2(H_2O)_2(ZnW_9O_{34})_2]$ in phosphate buffer at pH = 8.0 using pulsed voltammetry. In 2008, simultaneously and independently, two groups reported the preparation of a tetraruthenium POM $\{Ru_4(\mu\text{-}OH)_2(\mu\text{-}O)_4(H_2O)_4[\gamma\text{-}SiW_{10}O_{36}]\}^{10-}$ (Ru_4POM) as a high-efficient water oxidation catalyst.[44] The Ru_4POM species has also been extensively studied in light-driven water oxidation, which is an interesting approach to enhance the photocatalytic performances of POMs by coupling this type of catalyst with efficient photosensitizers. One of the most fascinating examples in this field is the assembled system containing the Ru(II) tetranuclear dendrimeric photosensitizer $[Ru\{(\mu\text{-dpp})Ru(bpy)_2\}_3](PF_6)_8$ (dpp = 2,3-bis(2′-pyridyl)pyrazine)[45] and a POM.[46] This system was tested for light-driven water oxidation in phosphate buffer with $Na_2S_2O_8$ and Na_2SO_4 as sacrificial oxidants. Very good performances were registered with a photoreaction quantum yield of 0.3 (excitation wavelength 550 nm), which means that 60% of the photons absorbed was used for oxygen production. This interesting value was achieved due to the fast hole scavenging, which prevented the decomposition of the antenna system. In 2019, an 'artificial quantasome' was reported, which was specifically designed by the template association of light-harvesting perylene bisimides with the polyoxometalate WOC, Ru_4POM.[47] The resulting $[PBI]_5Ru_4$POM complex, taking advantage of the electrostatic interactions and hydrophobic properties of the molecular building blocks, showed interesting oxygen evolution in the presence of the persulfate anion as a sacrificial agent.

An important example of a POM for water oxidation is $[Co_4(H_2O)_2(PW_9O_{34})_2]^{10-}$, which was reported in 2014 by Hill and group.[48] Hill tested its catalytic activity for the water oxidation reaction using $[Ru(bpy)_3]^{3+}$ as the oxidant. This system achieved a yield (4 $[O_2]/[Ru(bpy)_3]^{3+}$) of about 70% ± 5%[49] and an outstanding TOF in the range of 1600–2200 s^{-1}. A system for photocatalytic water oxidation was assembled using $[Co_4(H_2O)_2(PW_9O_{34})_2]^{10-}$ to act as the catalyst, $[Ru(bpy)_3]^{2+}$ as the photosensitizer and $Na_2S_2O_8$ as the sacrificial electron acceptor. Many investigations were conducted to study the stability of this complex. This POM was also unchanged after photocatalytic water oxidation, confirming its excellent features.

Another interesting paper reported a study about the catalytic efficiency of POMs with a huger number of atoms,[50] where $[Co_9(H_2O)_6(OH)_3(PW_9O_{34})_3]^{16-}$,[51] $[Co_6(H_2O)_{30}\{Co_9Cl_2(OH)_3(H_2O)_9(SiW_8O_{31})_3\}]^{5-}$ (ref. 52) and $[\{Co_4(OH)_3PO_4\}_4(PW_9O_{34})_4]^{28-}$ (ref. 53) were tested for the water oxidation reaction using $Na_2S_2O_8$ as the sacrificial electron acceptor and $[Ru(bpy)_3]^{2+}$ as the photosensitizer in phosphate buffer at pH 8. These complexes, due to their polyanionic nature, could interact with $[Ru(bpy)_3]^{2+}$, associating in ion pairs that enhance the efficiency of the system.

The mechanistic studies showed that the three systems investigated do not act in the same way. The cluster with 9 Co units can be considered to be composed of three $\{Co_3(m\text{-}OH)_3(H_2O)_6\}$ triads linked together by two HPO_4^{2-} bridges and six external water molecules. The POM with 16 Co units is made up of four $\{Co_4(m\text{-}OH)_3\}$ distorted cubanes connected through the phosphate linkers. In these two catalysts, a mono-electron transfer occurs from the cobalt core. The POM with 15 Co units had a different structure, in which three $\{Co_3(\mu\text{-}OH)(H_2O)_3\}$ triads are bound with six $Co^{(II)}(H_2O)_5$ groups positioned on the surface of the POM. In this catalyst, overall oxidation from Co(II) to Co(IV) was shown. Moreover, this configuration facilitated the proton-coupled electron transfer of the water molecules in the core and the external units. These considerations can explain the better performance of the latter complex than other ones analyzed and the great values of TON and TOF reported. Recently, molybdenum-based polyoxometalates containing mono and dicobalt(III) catalyst cores, $[CoMo_6O_{24}H_6]^{3-}$ and $[Co_2Mo_{10}O_{38}H_4]^{6-}$, were also investigated

as photocatalysts in the presence of $Na_2S_2O_8$ as the sacrificial electron acceptor and $[Ru(bpy)_3]^{2+}$ as the photosensitizer in borate buffer solution at pH 8. In this case, the presence of two cobalt centers did not increase the photocatalytic performances.[54] Indeed, in the case of $[CoMo_6O_{24}H_6]^{3-}$, there is a O–O coupling among the oxygen atoms in the structure, leading to an increase in its photocatalytic performances.[55]

Other earth abundant-based POMs have been studied, and among them, those containing manganese are of particular interest. In 2017, Zheng reported a study on photocatalytic water oxidation using $[Mn_3(H_2O)_3(SbW_9O_{33})_{12}]^{12-}$ as the catalyst at different concentrations.[56] This species, formed by two identical $Na_9[SbW_9O_{33}]$ Keggin portions, was firstly reported by Krebs.[57] Tests were conducted using $[Ru(bpy)^3]^{2+}$, $Na_2S_2O_8$ as the sacrificial oxidant and sodium borate buffet (pH 9). The best performance was recorded with a catalyst concentration of 10 mM (O_2 yield of 13.2% corresponding to a TON of 103). Exceeding this amount of catalyst led to a decrease in the efficiency of the system due to the formation and subsequent precipitation of the couple Dye-POM. After the photocatalytic experiments, the catalyst was reused to run other experiments and it was observed that the O_2 yield decreased from 13.2% to 8.0%. The robustness of this catalyst towards hydrolysis and oxidation was tested in different ways and the results of these measurements confirmed the high stability of this POM.

Another earth abundant metal that can form polyoxometallates able to catalyze light-driven water oxidation is vanadium. The first attempt reported in the literature[58] is related to the $[(V^{IV}{}_5V^{V}{}_1)O_7(OCH_3)_{12}]^-$ species.[59]

The peculiarity of this cluster is that the polyoxometalate framework is the active catalytic center itself, while the polyoxometalate is usually a scaffold used to stabilize the metal, acting like the actual catalyst. This species was tested as a light-driven water oxidation catalyst in a system with $[Ru(bpy)^3]^{2+}$ as the photosensitizer and $Na_2S_2O_8$ as the sacrificial oxidant in phosphate buffer at pH 7. Under these conditions, the system reached a photochemical quantum yield for O_2 production of 0.2 (this is a very high value considering that the theoretical yield is 0.5 because the absorption of two photons is needed to obtain one O_2 molecule). The rate constant of the hole-scavenging reaction (the electron transfer between the catalyst and the oxidized photosensitizer) was also determined and the calculated value is 2.5×10^8 M^{-1} s^{-1}. Furthermore, electrochemical water oxidation experiments clarified that $[(V^{IV}{}_5V^{V})O_7(OCH_3)_{12}]^-$ is not convert into vanadium oxides during the reaction, and thus it is an homogeneous catalyst itself.

2.4 Cubane-like catalysts

An interesting research line focuses on the development of water oxidation catalysts mimicking the oxygen evolving center (Mn_4CaO_5) of Photosystem II, which contains an Mn_3CaO_4 cubane structure.[60] Many attempts have been made to reproduce the design and the performances of this species using earth abundant metal.

One of the most notable, which appeared recently in the literature, is $[Cu_8(dpk{\cdot}OH)_8(OAc)_4](ClO_4)_4$ (dpk·OH = the monoanion of the hydrated, gem-diol form of di-2-pyridyl ketone).[61]

This structure, **12** in Fig. 8, is formed by two $[Cu(II)_4O_4]$ units linked by two acetate groups. It was used as a catalyst for water oxidation using $[Ru(bpy)_3](ClO_4)$ as the photosensitizer and $Na_2S_2O_8$ as the sacrificial electron acceptor in a borate buffer solution at pH 9. The reported results showed an oxygen yield of 38%, TON of 178 and TOF of 3.6 s^{-1}. Cyclic voltammetry, UV-vis absorption spectrometry, capillary electrophoretic analysis and other techniques were used to exclude the possibility that the cubane catalyst was not the active species but it decomposed into CuO_x. The results of these investigations confirmed that $[Cu_8(dpk{\cdot}OH)_8(OAc)_4](ClO_4)_4$ acts as a homogeneous molecular catalyst itself.

A cubane catalyst for water oxidation can also be coupled with photosensitizers to build a more complex and efficient supramolecular species. One important example in this field was designed and studied by Sun and coworkers in 2014.[62] They assembled $Co_4O_4(OAc)_4(py)_4$ with $[Ru(bpy)_2$ (4-methyl-4′-carboxy-bpy)] (see **13** in Fig. 8) to enhance the electron transfer between the two components of the system. This species was tested as a catalyst for water oxidation in a system composed of $NaHCO_3$ buffer at pH 7.0 containing and persulfate as the sacrificial oxidant. The reported TOF was 0.4 min^{-1}, which is much greater that showed by an analogous system in which the cubane unit is not linked to the photosensitizer. The better result of the former is due to the greater stability of the photosensitizer, easily transferring electrons intramolecularly to the cubane, thus avoiding one of the principal degradation pathways. Another system studied was a macrocycle constituted by two cubane units alternating with two photosensitizers (**14** in Fig. 8). This structure displayed a better performance than the linear structure with a TOF of 1.4 min^{-1} and five times greater

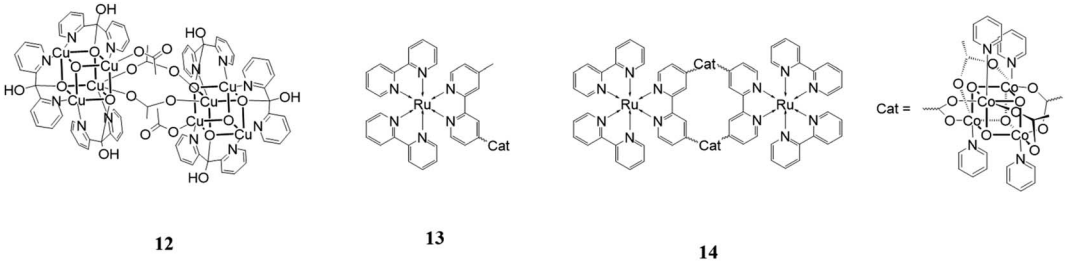

Fig. 8 Chemical structures of cubane catalysts.

O_2 production. This data can be explained by the additional stability given by the macrocyclic configuration.

A hypothesis sustained by some researchers involves considering that cubane catalysts are not molecular catalysts themselves but are just a precatalyst that turns into oxides, which act as heterogenous catalysts. Scientists have been debating for a long time about the real catalytic species and a study conducted in 2015 finally answered this question, clarifying that the catalytic activity is conducted by a molecular species.[63] In this paper, researchers conducted many experiments on $[Co_4O_4(OAc)_4(py)_4]$ (OAC = acetate, py = pyridine),[64,65] which they used as an example for all the family of Co-cubanes. In this structure, the alle metal centers are Co(III), cat in Fig. 8.

The test reported the enhanced efficiency of this catalyst with an increase in aging time, which may due to the formation of a more active species. A hypothetic pathway is the hydrolysis of the compound and the consequent release of the Co aqua ions, but ^{31}P-NMR denied this explanation. Kinetic investigations reported a more efficient electron transfer from this new species to $[Ru(bpy)_3]^{3+}$ (hole scavenging), which is about 40 times faster than the same process from $[Co_4O_4(OAc)_4(py)_4]$ to $[Ru(bpy)_3]^{3+}$. The great velocity of regeneration of the photosensitizer led to the greater stability of the latter and increased catalytic performance of the system. The photocatalytic system under illumination was also studied using continuous-wave EPR. This analysis showed the formation of Co(IV) in the metallic core due to the photogenerated $[Ru(bpy)_3]^{3+}$. After 20 min of irradiation, the formation of a Co(II), concomitant with a decrease in the Co(IV) signal, was registered. This new species could be the resting state of the active species originating from the cubane.

3. CO_2 reduction

The mass consumption of "fossil fuels" has led to an increasing amount of atmospheric CO_2, causing serious environmental problems, *e.g.* global warming[66] and the greenhouse effect.[67,68] These problems have affected our planet for over a century. In this case, reducing CO_2 to obtain energy-rich chemicals, such as CO and HCOOH, can be a solution to shortage of carbon resources environmental problems.[69] Although CO_2 may be reduced through a one-electron process (eqn (4)), this reaction requires a very low potential (−1.9 V *vs.* SHE) to be realized, becoming effectively of no interest for the intended purpose.

$$CO_2 + e^- \rightarrow CO_2^{\cdot -} \quad E^\circ = -1.9 \text{ V } vs. \text{ SHE(at pH 7)} \qquad (4)$$

$$CO_2 + 2H^+ + 2e^- \rightarrow CO + H_2O \quad E^\circ = -0.52 \text{ V } vs. \text{ SHE (at pH 7)} \qquad (5)$$

$$2CO_2 + 2e^- \rightarrow CO + (CO_3)^{2-} \quad E^\circ = -0.64 \text{ V } vs. \text{ SHE (at pH 7)} \qquad (6)$$

$$CO_2 + 2H^+ + 2e^- \rightarrow HCOOH \quad E^\circ = -0.61 \text{ V } vs. \text{ SHE (at pH 7)} \qquad (7)$$

Conversely, the CO_2 reduction reactions that involve two-electron transfer processes (eqn (5)–(7))[70] can be effectively employed at significantly more positive potentials with respect to eqn (4), and also the two-electron product of CO_2 reduction are mainly carbon monoxide (CO) and formic acid (HCOOH). CO can be easily converted into liquid hydrocarbon by the Fischer–Tropsch synthesis;[71] however, formic acid has been investigated as a potential H_2 storage material in recent years, given that it is liquid at room temperature and can be easily converted to CO_2 and H_2 with suitable catalysts under moderate conditions[72] or used directly as fuels in direct formic acid fuel cells (DFAFCs).[73]

The catalytic cycle to reduce CO_2 may follow two different paths, depending on whether the excited photosensitizer undergoes a reductive quenching process or an oxidative quenching process. The starting step of each pathway is the absorption of a photon by the PS subunit with the formation of the excited state of the photosensitizer. In the reductive mechanism, a sacrificial electron donor reduces the excited photosensitizer, and subsequently the reduced photosensitizer transfers the electron to the catalyst to collect negative charges (Fig. 1b). In the oxidative mechanism, excitation of the photosensitizer is followed by a charge separation process, leading to the formation of the oxidized form of photosensitizer and the reduced form of the catalyst; eventually, the photosensitizer is restored by an electron transfer process that involves a sacrificial electron donor (Fig. 1b).

The first studies on photocatalytic CO_2 reduction were conducted by Lehn and co-workers in the early 1980s. They employed *fac*-Re(bpy)$(CO)_3$Cl complexes as photocatalysts[74,75]. This type of compound has been proven to be selective and efficient for CO_2 reduction but showed some drawbacks such as limited absorption in the UV region, low abundance of rhenium, low turnover number and necessary presence of an electron donor.[76] Thus, to maximize the efficiency of photocatalysis, it is crucial to introduce a sensitizer to the previously known catalysts. To use visible light as best as possible, in recent years the aim of research has been the introduction of a link (a bridging ligand) between the photosensitizer and the catalyst. Regarding this goal, the photocatalytic reduction of CO_2 is performed using multinuclear metal complexes combined with redox photosensitizers (PS), which can mediate photoinduced electron transfer from a reductant (D) to a catalyst, and the catalyst (C) itself, the so-called supramolecular photocatalyst, has been extensively investigated.[77,78]

In supramolecular photocatalysts, faster electron transfer occurs between the PS and C subunits, which leads to an improvement in the performances of these systems with respect to the separated species in solution due to the increase in the photocatalysis speed and higher durability of the photosensitizer subunit, given that the unstable intermediate state is consumed faster than in separated mixed systems. The photocatalytic performances with their experimental conditions of all the catalyst metal complexes suitable for CO_2 reduction reported in this review are summarized in Table 2.

3.1 Integrated systems: multinuclear species with different functionalities

One of the advantages of multinuclear complexes is the possibility to link various units with different functions within the

Table 2 Photocatalytic performances of the reported catalysts for CO_2 reduction

Catalyst	TON	TOF	Experimental conditions
17	671	11.6 min^{-1}	HCOOH formation BNAH as sacrificial agent DMF/TEA (4 : 1, v/v)
21	315	—	CO formation BNAH as sacrificial agent DMF solution
22	286	—	CO formation BNAH as sacrificial agent DMA/TEOA(5 : 1, v/v)
31–34	—	12–29 h^{-1}	CO formation TEOA as sacrificial agent CH_3CN as solvent
35	60	21 h^{-1}	CO formation TEOA as sacrificial agent CH_3CN as solvent
Co(II) cryptate	16 896	0.47 s^{-1}	CO formation TEOA as sacrificial agent CH_3CN/H_2O (4 : 1, v/v) PS: $[Ru(phen)_3](PF_6)_2$
Co(II)–Zn(II) cryptate	65 000	1.8 s^{-1}	CO formation TEOA as sacrificial agent CH_3CN/H_2O (4 : 1, v/v) PS: $[Ru(phen)_3](PF_6)_2$
Cu(I)–Co(II) cryptate	2305	—	CO formation TEOA as sacrificial agent CH_3CN/H_2O (4 : 1, v/v) PS: $[Ru(phen)_3](PF_6)_2$
36	829	—	CO formation Phenol as sacrificial agent CH_3CN as solvent
37	766	—	HCOOH and CO formation (60 and 28% selectivity) CH_3CN as solvent PS: $[Ru(phen)_3](PF_6)_2$
38	255		See ref. 96
Ni(II) S_2N_2-type complex	120	0.87 min^{-1}	See ref. 98
$[Co_5(btz)_6(NO_3)_4(H_2O)_4]$	2748		CH_3CN as solvent TEOA as sacrificial agent PS: $[Ru(bpy)_3]Cl_2$
$[CoZn(bpbp)(CH_3COO)_2](CH_3COO)$	6680	0.19 s^{-1}	CO formation CH_3CN/H_2O (4 : 1, v/v) TEOA as sacrificial agent PS: $[Ru(phen)_3](PF_6)_2$
$[Fe_2Na_3$(1,2-oxo-4-hydroxyanthracene-9,10-dione$)_6](TBA)_3$	2625	—	CO formation (91% selectivity) BIH as sacrificial agent DMF as solvent
39	14 956	276 min^{-1}	CO formation TEA as sacrificial agent PS: CzIPN

system with topological control, usually resulting in better overall stability and predetermined photosensitizer/catalyst ratios (due solely to the synthetically-determined structure of the system).

Ishitani and co-workers[79] synthesized and studied several Ru(II) multinuclear complexes (Fig. 9), where based on the ligands, the Ru(II) centers may act as catalytic subunits (through fragments of the type of $[Ru(dmb)_2(CO)_2]^{2+}$) or as photosensitizer subunits ($[Ru(dmb)_3]^{2+}$). They synthetized and investigated four different integrated systems by varying the number of photosensitizers or catalyst moieties, including species 15 (one catalyst and one sensitizer moiety), species 16 (one sensitizer and two catalyst subunits), species 17 (one catalyst and two photosensitizer moieties) and species 18 (one photosensitizer and three catalyst subunits). Studying the CO_2 photocatalytic reduction, it was observed that the outcome product of the catalytic cycle is strongly dependent on the ratio between the catalyst and the photosensitizer units, resulting in the favorable formation of HCOOH with a high Ru(photosensitizer)/Ru(catalyst) ratio, and *vice versa*, obtaining CO as the major product with a low Ru(photosensitizer)/Ru(catalyst) ratio. The experiments were performed in a mixture of DMF/TEOA (v/v =

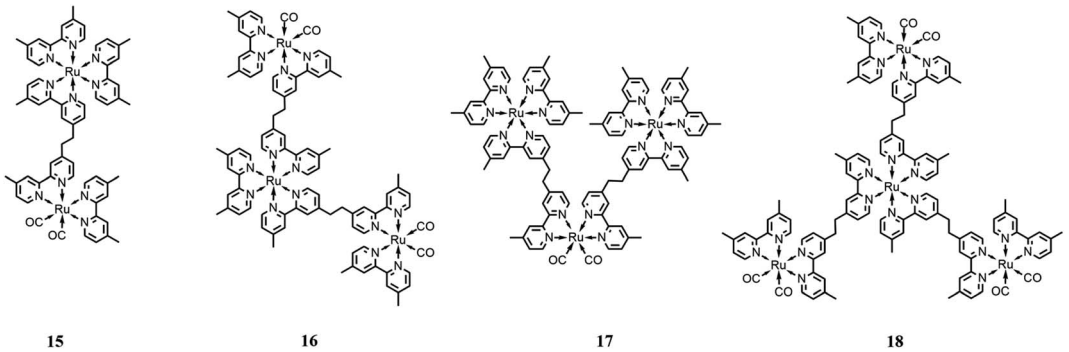

Fig. 9 Different integrated systems with the Ru(II)-based photosensitizer and Ru(II)-based catalysts. Charge is omitted for clarity.

4 : 1), with BNAH as the sacrificial reductant, under irradiation at 480 nm. The authors highlighted the important role of TEOA in the catalytic cycle, which was also supported by previous works.[80] Specifically, TEOA does not serve as an electron donor, but it acts as proton-acceptor for the one-electron oxidation process involving BNAH, simultaneously suppressing the back-electron transfer process between the reduced photosensitizer and the oxidized BNAH. In addition, it results in the more favorable reduction of CO_2 to HCOOH. It was reported that the most efficient photocatalytic system was the complex formed by a single Ru(catalyst) subunit bound to two Ru(photosensitizer) subunits, promoting the formation of HCOOH with a TON of 671 and TOF of 11.6 min^{-1}.

Rieger and co-workers[81] reported a trinuclear complex consisting of a photosensitizer subunit, $[Ru(dmb)_3]^{2+}$, bound to two catalyst subunits, $[Re(dmb)(CO)_3Cl]$ (**21** in Fig. 10). It was studied in comparison with model systems incorporating one Ru(II) center and two Re(I) centers with different bridging modes (**19** and **20** in Fig. 10). The performance of these trinuclear mixtures was assessed in the photocatalytic reduction of CO_2 to examine the influence of covalent bounds connecting each of the individual complexes. The catalytic performances were tested in a DMF solution, with BNAH as the sacrificial electron donor, assisted by TEOA, under 520 nm irradiation, obtaining a TON of 315 for CO. The authors found that the photocatalytic performance of the trinuclear complex is enhanced in comparison with

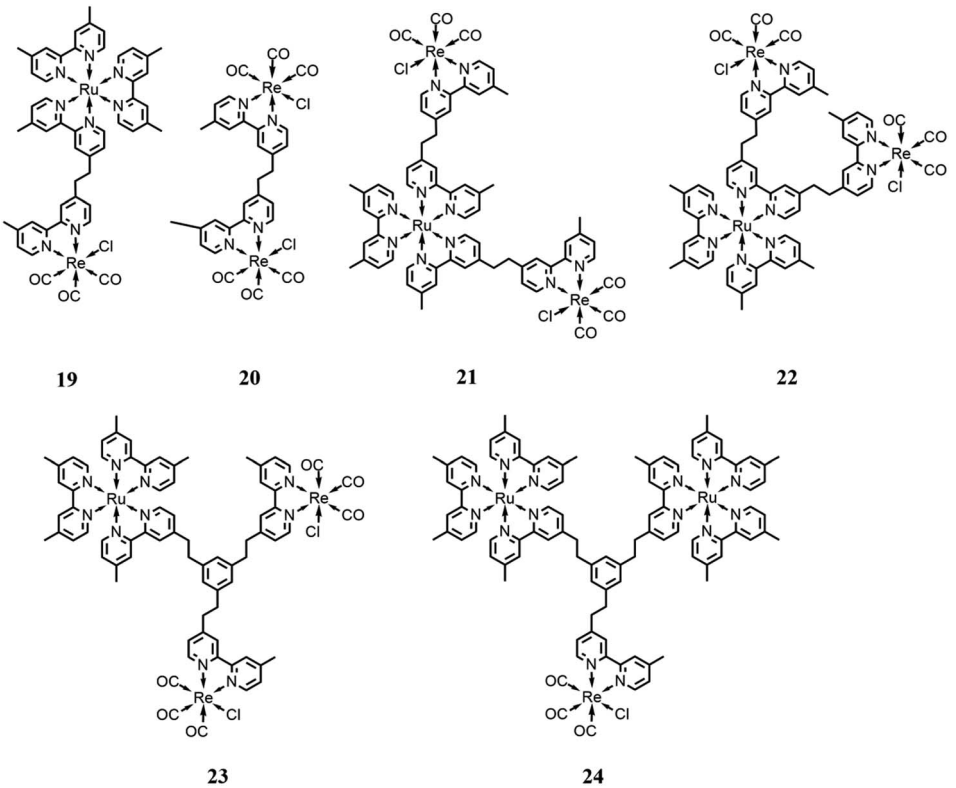

Fig. 10 Integrated systems with different ratios and bridging ligands with the Ru(II)-based photosensitizer and Re(I)-based catalysts. Charges are omitted for clarity.

the model systems, facilitating a faster CO_2 reduction due to a dinuclear reduction mechanism. Moreover, the covalent bounds between the subunits enable intramolecular electron transfer processes, which lead to a shortened lifetime of the one-electron reduced photosensitizer, making the complex less susceptible to deactivation caused by photobleaching resulting from the excitation of the reduced photosensitizer. Besides, the covalent linkage of the system enabled the Re(I) subunits to act as light antennae, improving the system in its entirety.

Ishitani and co-workers[82] designed and synthesized a trinuclear complex consisting of an Ru(II)-based photosensitizer subunit linked to two Re(I) catalyst subunits through ethylene chains (**22** in Fig. 10) and compared its photocatalytic behavior with related mono- and dinuclear Ru- and Re-based complexes, in solution with defined molar ratios. CO_2 photoreduction tests were conducted in a DMA/TEOA solution (v/v = 5 : 1) with BNAH as the sacrificial reductant and an irradiation wavelength of >500 nm. In comparison with the model systems, the trinuclear complex showed enhanced behavior and the decomposition rate of the Ru unit in the **21** system during the photocatalytic reaction occurred at a slower pace, with a TON of 286 and CO formation selectivity of 90%. The better stability, and thus the higher selectivity for CO evolution, was correlated to the suppression of the photochemical ligand substitution, which appears to occur only to the detriment of mononuclear Ru-units, while leaving the ruthenium subunits of the trinuclear and dinuclear complexes intact. This was also associated with the lower localization of the photochemically added electron in the ruthenium subunit caused by the electron transfer process to the two rhenium subunits.

Other developments by the same research group consisted of increasing the distance between the photosensitizer and the catalyst subunits by using different bridging ligands compared to the simplest alkyl chain reported to date in the literature.[83] In particular, they used a tris-chelating polypyridine ligand composed of a phenylene ring connected at the 1, 3, 5 positions to the 2,2′-bypiridine moieties by an ethylene chain. This bridging ligand is suitable for the synthesis of trinuclear complexes with different ratios between the photosensitizer (based on $Ru(dmb)_3$-type chromophore) and catalyst (based on $Re(dmb)(CO)_3$-type) subunits (**23** and **24** in Fig. 10), respectively. All these systems showed a negligible electronic interaction between the subunits in the ground state, and thus the metal subunits also presented their own photophysical and redox properties in the supramolecular assemblies. These systems were tested in DMA/TEOA solution (v/v = 5 : 1) with BNAH and BIH as the sacrificial electron donor and an LED (530 nm, 4 mW) as the light source. The results showed that the assemblies presented quite efficient visible light-induced catalytic CO formation with high a turnover number, selectivity and durability when BIH was employed as the sacrificial agent. The better performance obtained by the use of BIH can be rationalized because BIH donates both electrons to the photocatalytic systems required for CO_2 reduction.[16]

The results also showed the better performances in terms of selectivity and turnover number of the system with 2 catalytic and 1 photosensitizer subunits compared with the system with only 1 catalyst and 2 photosensitizers.

Further investigations[84] were performed on these systems, where on the catalytic subunits contained the CO_2TEOA adduct (known to be an effective catalytic subunit) instead of chloride, which showed an increase in the turnover number and selectivity. This result could be rationalized considering the different distributions of the one-electron reduced form of the supramolecular photocatalysts on the Ru-subunit(s) (leading to decreased CO formation due to a poisoning ligand loss process) and on the Re-subunit(s) and to the presence of chloride ions in solution (inevitable for the species with a chloride ligand), which could interfere with the formation of the CO_2TEOA adduct, a requisite for CO-forming catalysis. These results also confirmed the better performance of the 2 : 1 catalyst-photosensitizer assembly analogously to that observed for the precursor species with the chloride ligand.

Inagaki and co-workers[85] achieved the photoinduced hydrogenation of CO_2 using a trinuclear iridium hexahydride complex (**26** in Fig. 11) as a photo-switchable catalyst. Each Ir center is also complexed by a diphosphine ligand, which acts as a photosensitizer. For comparison, two other analogue complexes were also studied (**27** and **29** in Fig. 11). Their photocatalysis performances were evaluated in MeOH, under LED irradiation at 395 nm, in an atmosphere of CO_2/H_2 (1 : 1 ratio) and a total pressure of 10 atm. Tests were also performed under

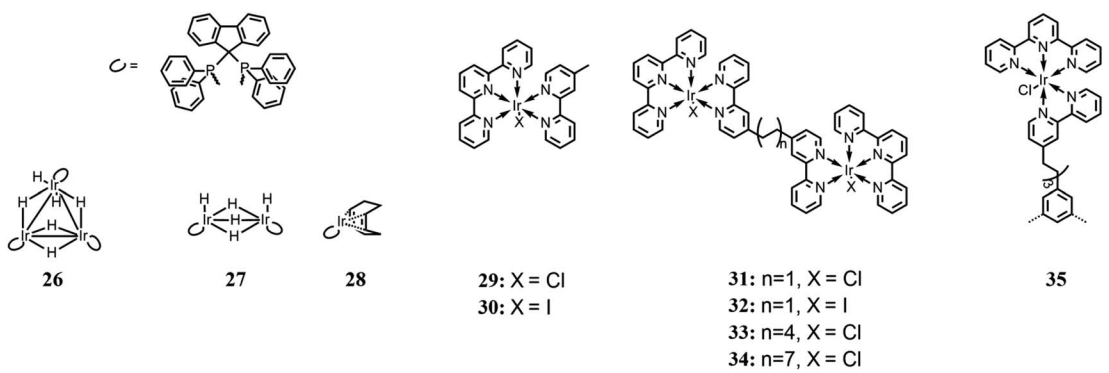

Fig. 11 Iridium-based photocatalytic systems. Charge and counter anions are omitted.

dark and light conditions to evaluate the switchability of the complexes. Among the several bases used to achieve HCOOH formation, DBU, thanks to its high basicity, exhibited the highest activity. Overall, the trinuclear complex showed the best catalytic performance, which was enhanced by light irradiation. The authors reported that irradiation facilitated the H_2 activation process, which is considered one of the rate-determining steps in the involved reactions and confirmed under a D_2 atmosphere by evaluating the H–D exchange reaction. It was explained that the possible effect of light could be the dissociation of the coordinated hydrides, thus leaving unsaturated coordination sites for complexation by CO_2. In fact, the CO_2 insertion process was also found to be enhanced by light irradiation.

A different type of integrated systems is shown below, which was structured not as connected subunits, with some acting as a catalyst and others as a photosensitizer, but as multinuclear complexes, where each unit can act not only as a catalyst but also as a photosensitizer.

Herdtweck and co-workers,[86] based on the work of Ishitani *et al.*,[87] designed several dinuclear Ir(III) complexes, whose metallic centers are connected through bis(2-phenylpyridin-4-yl) bridging ligands (from **31** to **34** in Fig. 11). The four dinuclear complexes differ from each other based on the coordinated halides and/or the length of the bridging ligand. Catalytic activity for CO formation was investigated under a 450 nm light source, in CH_3CN, with TEOA as sacrificial reductant. No photosensitizer was used because the iridium complexes themselves can act as one. In comparison with analogous Ir(III) mononuclear complexes reported in the same work and shown in Fig. 11 (**29** and **30** respectively), the stability of the dinuclear systems appeared to be highly improved, and among the four complexes, TON values in the range of 80–135 were achieved, calculated per molecule of catalyst, and TOF in the range of 12–29 h^{-1}. The difference of catalytic capabilities was attributed to the length of the bridging ligand, which only enabled a weak interaction between the Ir(III) centers for the shortest alkyl chains and no interaction for the longest ones, and to steric hindrance. Besides, differently from the previous work by Ishitani, where the catalyst deactivation was attributed to dimerization processes,[87] the authors considered these processes or their minor relevance and believed that the deactivation may be ascribed to the oxidation products of TEOA.

Rieger and co-workers,[88] continuing the work of Herdtweck *et al.*,[86] synthesized a trinuclear Ir(III) complex, whose properties and photocatalytic behavior were compared with mono- and dinuclear analogue complexes (**35** and **31** in Fig. 11), respectively. The authors reported the selective reduction of CO_2 to CO with no other reduction products formed. Photocatalysis tests were performed in CH_3CN, with TEOA as the sacrificial electron donor, by irradiating at 450 nm, and similar to the previous work,[85] no photosensitizer was added. Among the three complexes, the highest TON value (60, calculated per Ir(III) center) was obtained for the trinuclear complex, with a TOF of 21 h^{-1}. Because both the TOF and quenching constant are situated between the respective values of mono- and dinuclear complexes, it is assumed that there is a strong correlation between the photocatalytic performance and the effect of intramolecular quenching.

3.2 Cryptands

Metal cryptate complexes have received some attention in the field of photocatalysis given that their space orientation allows synergistic catalysis between the coordinated metal centers, leading to a more efficient CO_2 reduction with respect to mononuclear systems in terms of efficiency, yield and selectivity.

Lu and co-workers[89] realized a dinuclear Co(II) cryptate to achieve the photocatalytic reduction of CO_2 to CO, investigating the kinetic properties to evaluate the synergistic effect between the two cobalt metal centers. It was found that only one of the two Co(II) ions acts as the actual active site for the catalytic process; the second Co(II) ion reduces the energy barrier for CO_2 reduction, with respect to an analogous mononuclear compound, by facilitating the removal of the hydroxyl group in the C–OH fragment that is formed within the catalytic process. These results were supported by the experimental analysis and DFT calculations. In a mixture of CH_3CN/H_2O (v/v = 4 : 1) and under 450 nm LED light irradiation, the authors reported a TON of 16 896 and a TOF of 0.47 s^{-1}, with a CO selectivity of 98%. $[Ru(phen)_3](PF_6)_2$ was used as the photosensitizer and TEOA as the sacrificial reductant.

Lu and co-workers[90] continued their work studying a dinuclear heterometallic cryptate based on a Co(II) ion and a Zn(II) ion. This complex is equivalent to the homonuclear one studied previously.[88] In reference to their precious work, the authors reported an increase in the photocatalytic performances, operating under the same conditions.[88] This catalyst achieved CO_2 reduction with a TON of 65 000, TOF of 1.8 s^{-1} and selectivity of 98%. The increased efficiency of the process was attributed to the stronger binding affinity of the Zn(II) ion to the hydroxyl group compared to the Co(II) ion, thus enhancing the whole process. Referring to the mechanism, the Co(II) center was reported to act as the actual catalyst site, whereas the Zn(II) center is the assistant catalyst site.

Martinho and co-workers[91] realized three dinuclear Co(II) octaazacryptate catalysts, which have well-known photophysical behavior, and studied the influence of the electron-withdrawing and -donor effect of the functionalized in the aromatic rings. They reported that the photocatalytic reduction of CO_2, under blue visible light (492–455 nm), was only successful using $[Ru(phen)_3](PF_6)_2$ as the photosensitizer and TEOA as the sacrificial electron-donor, using a solution of CH_3CN/H_2O (v/v = 4 : 1) as the solvent. This behavior was attributed to the stronger oxidizing power of the photosensitizer/sacrificial agent pair compared to the other ones tested. Beyond that, it was reported that at a low catalyst concentration, solely CO was produced but increasing the catalyst concentration or the light-exposure time (30 h), a mixture of CO and CH_4 was evolved. A TON of 27 311, TOF of 0.25 s^{-1} and CO selectivity of 92% were achieved.

Su and co-workers[92] studied a cryptate trinuclear Re(I) catalyst. A higher catalytic performance compared to the analogous mononuclear Re-bpy complex was recorded, which was

attributed to (i) the easier adsorption of CO_2 and, consequently, the easier contact between catalytic sites and substrate due to the structure of the cryptands themselves and (ii) to the bridging ligands, which are capable of achieving a faster electron transfer process (point supported by cyclic voltammetry studies). Photocatalysis tests were conducted in a DMSO/H_2O solution by using $Ir(ppy)_3$ as the photosensitizer and BIH as the sacrificial electron donor, with an LED light source at a wavelength of >420 nm.

Apfel and co-workers[93] synthesized an asymmetric ($[(CH_2)_2$-$SCH_2(m\text{-}C_6H_4)CH_2NH(CH_2)_2]_3N$) dinuclear cryptand based on Cu(I) and Co(II) centers based on the work of Lu *et al.*[89] and taking inspiration from CO_2-converting enzymes to opt for a sulphur-rich coordination site. Photocatalytic experiments were performed in CH_3CN/H_2O (v/v = 4 : 1) with $[Ru(phen)_3](PF_6)_2$ as the photosensitizer and TEOA as the sacrificial electron donor, under an LED light (450 nm). Photoinduced reduction tests resulted in a TON of 2305 and CO selectivity of 98%. The authors emphasized the importance of the synergistic effect arising from the presence of the two metal centers, which was proven by comparison with analogue mononuclear complexes and computational studies. The importance of the metal–metal distance was also specified: in fact, increasing this distance led to a lower synergistic effect, resulting in a process catalyzed only by the Co(II) center.

3.3 Multinuclear catalysts using a xanthene bridge

Similarly to metal cryptates, dinuclear complexes based on a molecular structure have been reported, enabling synergistic catalysis, namely, two chelating moieties connected by a xanthene bridge.

Robert and co-workers[94] reported a dinuclear Co(II) bisquaterpyridine complex (**36** in Fig. 12) capable of the visible light-induced selective formation of formate ion or CO. The solvent used for the photocatalysis tests was CH_3CN. Although the authors reported that DMF is a better solvent to be used for formate production, they also cited studies where it was affirmed that traces of water or amine may cause hydrolysis products that can poison the catalytic cycle,[95] and thus they preferred CH_3CN. Besides, several combinations of photosensitizers and sacrificial reductants were involved under 460 nm LED irradiation. It was found that adding phenol, a weak acid, to the solution it was possible to obtain CO formation selectively; according to the authors, this dual activity is caused by the synergy of the two Co centers, which are capable of controlling the two-electron/two-proton CO_2 reduction. In the absence of weak acid, formate with a selectivity of 97% and a TON of 821 were obtained; conversely, in the presence of weak acid, CO was highly produced with a selectivity of 99% and TON of 829. Mechanistic studies were also conducted by DFT calculations to propose the catalytic cycle scheme.

Robert and co-workers[96] continued their previously reported study[93] using an analogue dinuclear Cu(II) bisquaterpyridine complex (**37** in Fig. 12) in CH_3CN under irradiation at 420 nm. In this study, a fundamental synergy was also found between the two metallic centers, which in the presence of water as a proton donor, generates a bridging metal-hydride intermediate (M–H–M), thus achieving photoinduced CO_2 reduction to formate ion. CO is also produced, derived from CO_2 forming an adduct with the reduced catalyst, which was restored following the reduction of CO_2 to CO. However, the amount of water did not seem to affect the selectivity of the catalyst, according to the authors, implying that the initial charge transfer steps to the catalysts limit the overall rate. A TON value of 766 was reported, with a selectivity of 60% for formate and 28% for CO, using $Ru(phen)_3^{2+}$ as a photosensitizer. The authors also reported a comparative study with an analogous mononuclear Cu complex (Fig. 10b), indicating that by using thus complex as a CO_2 catalyst, only CO is formed, and thus the authors hypothesized the presence of the above-mentioned bridging hydride.

Tschierlei and co-workers[97] studied a dinuclear Re(I) complex based on $Re(bpy)(CO)_3Cl$ units bound to each other through a xanthene bridge (**38** in Fig. 12). The authors previously reported a study focused on the related mononuclear complex ($Re(bpy)(CO)_3Cl$),[98] and found that a dimer of the mononuclear Re(I) complex is a crucial intermediate for CO_2 reduction to CO, and the studies were continued, investigating the aforementioned dinuclear Re(I) complex. Environmentally friendly photosensitizers were used, specifically $[Cu(xant)(bcp)](PF_6)$ and $[Ir(dFppy)_3]$. Besides, photocatalysis tests were performed using several sacrificial electron donors (TEA, TEOA and BIH) in various combinations. It was reported that the dinuclear complex exhibited better CO_2 activation in comparison with the mononuclear complex, with a higher TON of up to 45 times (255).

3.4 Catalysts based on earth abundant metals

Great efforts have also been devoted in the last decade to synthesizing complexes based on low-cost earth-abundant metals, *e.g.* Ni, Mg, Fe, Na, Zn and Co, to go beyond the use of noble metals, which are more expensive due to their low abundance and difficult extraction.

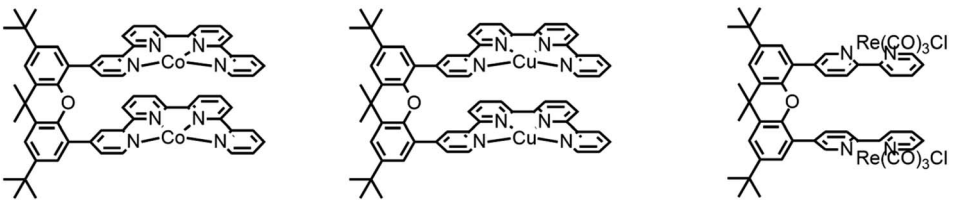

36 37 38

Fig. 12 Structures of different systems using the xanthene bridge.

Kojima and co-workers[99] synthesized an Ni(II) complex bearing an S_2N_2-type tetradentate ligand and two pyridine pendants, which may act as coordination sites for Lewis acids. In this instance, the two pyridine fragments coordinate with an Mg^{2+} ion, which enhanced the production of CO by photoinduced CO_2 reduction in comparison to the Ni(II) complex with no coordinated Lewis acid. The authors supported the idea that the Mg^{2+} ion greatly helps to trap CO_2, leading to easier CO_2–metal intermediate formation and efficient catalytic behavior even at a low CO_2 concentration. In addition to Mg^{2+}, they reported the dependence of CO evolution related to other Lewis acids (Li^+, Na^+, Ca^{2+}, Zn^{2+}, Sc^{3+} and Y^{3+}), but only Ca^{2+} and Zn^{2+} ions were capable of exhibiting photocatalytic behavior similar to that recorded for the Ni(II)–Mg(II) complex. All the photocatalysis experiments were performed in a mixture of DMA/H_2O (v/v = 9 : 1) under a 450 nm LED lamp, using $[Ru(bpy)_3]Cl_2$ as a photosensitizer and BIH as the sacrificial electron donor. In the case of the Ni(II)–Mg(II) complex, it was reported to show a TON of 120, TOF of 0.87 min^{-1} and a selectivity value for CO of 99.7%.

Su and co-workers[100] explored a pentanuclear Co(II) complex, $[Co_5(btz)_6(NO_3)_4(H_2O)_4]$, for CO_2 conversion to syngas (CO and H_2). Photocatalysis tests were carried out under a pure flux of CO_2 in CH_3CN, with $[Ru(bpy)_3]Cl_2$ as the photosensitizer and TEOA as the sacrificial reductant, under irradiation from a xenon lamp at 420 nm. Compared with a mononuclear cobalt complex with a similar structure, the syngas produced was 212 times higher, with a TON value of 2748 within 70 h. The catalytic cycle also showed the advantage of granting a wide adjustability of H_2/CO ratio by varying the solvent component and the amount of TEOA, ranging from 16 : 1 to 2 : 1. The good performance of the complex for syngas evolution was also confirmed for a diluted CO_2 flux. DFT calculation was also conducted, showing a low energy barrier for the formation of the photocatalytic intermediate, which supported the experimental evidence of the efficiency for CO_2 reduction.

Chen and co-workers[101] synthesized and studied the photocatalytic behavior a Co(II)–Zn(II) heterometallic dinuclear complex $[CoZn(bpbp)(CH_3COO)_2](CH_3COO)$ and a Co(II) homometallic dinuclear complex $[Co_2(bpbp)(CH_3COO)_2](CH_3COO)$ using $[Ru(phen)_3](PF_6)_2$ as the photosensitizer and TEOA as the sacrificial reductant, in several solvents and solvent mixtures, obtaining the best performance with CH_3CN/H_2O (v/v = 4 : 1) as the solvent. The irradiation was conducted for 10 h under a 450 nm LED light. The authors reported that both complexes acted efficiently as a catalyst for the photoinduced reduction of CO_2 to CO, highlighting that the heterometallic complex

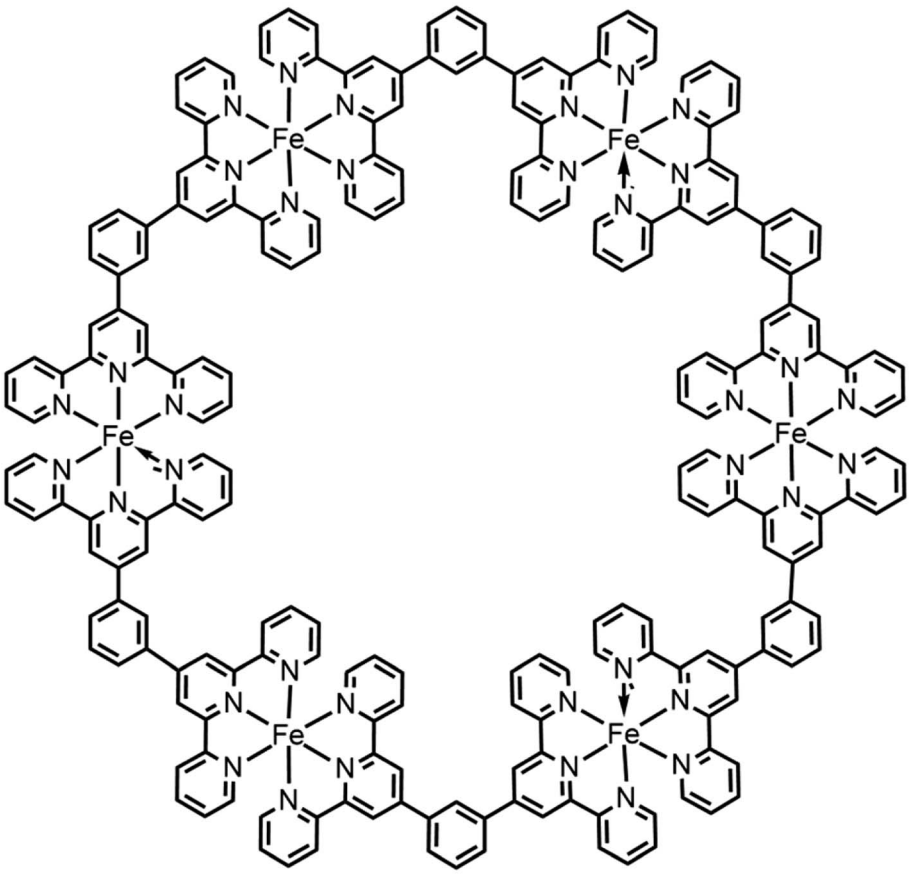

39

Fig. 13 Fe(II) macrocyclic catalyst for CO_2 reduction.

exhibited the best performances. Based on the DFT studies, they ascribed this result to the lower energy barrier related to the coordination for CO_2 from the heterometallic complex with respect to the energy barrier related to the homometallic coordination. In fact, they found that the Co center of the heterometallic complex showed a higher electron density than the Co centers of the homometallic complex, leading to the easier coordination of CO_2, which was the rate-limiting step. The TON, TOF and CO selectivity values were reported to be 6680, 0.19 s^{-1} and 98%, respectively, for the Co–Zn complex.

Han and co-workers[102] reported a heterometallic purpurin complex based on earth-abundant elements ($[Fe_2Na_3$(1,2-oxo-4-hydroxyanthracene-9,10-dione)$_6](TBA)_3$), which was capable of reducing CO_2 to CO under irradiation from a 450 nm light with no additional photosensitizer. In fact, photoinduced electron transfer was reported from the excited ligands to the iron centers, which acted as catalytic sites for CO_2 reduction. This system achieved a TON of 2625 and 91% selectivity for CO production in DMF, with BIH as the sacrificial electron donor.

Chao and co-workers[103] reported a cyclic complex based on six Fe(II) centers with terpyridine-based bridging ligands (Fig. 13).

They studied the catalytic performances by coupling the complex to 4CzIPN (an organic photosensitizer) and TEA as the sacrificial reagent, under irradiation from a white LED light (420–650 nm). This complex showed catalytic activity for CO evolution with a TON of 14 956, TOF of 276 min^{-1} and CO selectivity of 99.6%. The authors emphasized the importance of the ligands, given that they are redox-active, and consequently contribute significantly to CO_2 photoreduction. In fact, they demonstrated that the photosensitizer could reduce the terpyridine fragments, leading to an electron reservoir, and therefore achieving an easier and highly efficient CO_2 reduction process.

4. MOFs and COFs as multinuclear photocatalysts

Metal–organic frameworks (MOF) and covalent organic frameworks (COF), in particular show numerous interesting applications such as gas separation and absorption,[104] environmental treatment, catalysis[105] and energy conversion. In the last decade, a particular class of multinuclear catalysts for artificial photosynthesis is represented by MOFs and COFs.

MOFs exhibit a regular crystalline lattice, which is composed of metal ions or metal ion clusters and bridging organic linkers conveniently assembled, leading to a well-defined porous structure, which is the principal responsible for their interesting properties.[106] Also, COFs show a crystalline polymeric organic structure with high porosity, in which their building blocks are covalently linked in a giant covalent structure.[107] Due to the covalent nature of their intramolecular bonds, COFs present also high stability and high tunability of their properties by changing the building blocks and due to the diversity of their covalent linkage topology.[108] Indeed, MOFs and COFs are characterized by the tunability of their properties by changing their base components, offering the opportunity to increase their properties by anchoring active sites inside their pores.

To date, there are many reviews in the literature on the use of MOFs and COFs in photocatalytic water oxidation, CO_2 reduction[109] and the overall water splitting process[110] and this topic is too vast to be exhaustively debate here.

5. Conclusion

In the last few decades, many metal complexes with multiple catalytic subunits have been reported in the literature. The aim of this review was exploring catalysts for oxygen evolution and CO_2 reduction, which are composed of multinuclear metal centers. Herein, were discussed multinuclear systems with only catalytic centers and integrated systems with more than one catalytic subunit and photosensitizer moieties. In almost all the reported compounds, both in oxidation and reduction processes, according to the comparison with the homologous mononuclear species, it is possible to observe that there is an increase in stability, durability and overall photocatalytic performances in the presence of more than one active unit. Moreover, in integrated systems, the connection between the catalysts and the photosensitizers leads to a further increase in the photocatalytic performances.

Conflicts of interest

There are no conflicts of interest to declare.

Acknowledgements

This work was funded in part by a grant from the Italian Ministry of Foreign Affairs and International Cooperation (PGR project on Artificial Photosynthesis, collaboration Italy-Japan, Grant Number JP21GR09) and in part by European Union (NextGeneration EU), through the MUR-PNRR project SAMOTHRACE (ECS00000022).

Notes and references

1 J. Curtin, C. McInerney, B. Ó Gallachóir, C. Hickey, P. Deane and P. Deeney, *Renewable Sustainable Energy Rev.*, 2019, **116**, 109402.
2 B. Hawkins Kreps, *Am. J. Econ. Sociol.*, 2020, **79**, 695–717.
3 V. Scott, R. S. Haszeldine, S. F. B. Tett and A. Oschlies, *Nat. Clim. Change*, 2015, **5**, 419–423.
4 T. R. Karl and K. E. Treberth, *Science*, 2003, **302**, 1719–1723.
5 N. S. Lewis and D. G. Nocera, *Proc. Natl. Acad. Sci. U.S.A.*, 2006, **103**, 15729–15735.
6 H. Ahmad, S. K. Kamarudin, L. J. Minggu and M. Kassim, *Renewable Sustainable Energy Rev.*, 2015, **43**, 599–610.
7 J. Qi, W. Zhang and R. Cao, *Adv. Energy Mater.*, 2018, **8**, 1701620.
8 C.-H. Liao, C.-W. Huang and J. C. S. Wu, *Catalysts*, 2012, **2**, 490–516.
9 S. Zhang, Q. Fan, R. Xia and T. J. Meyer, *Acc. Chem. Res.*, 2020, **53**, 255–264.

10 X. Li, S. Wang, L. Li, Y. Sun and Y. Xie, *J. Am. Chem. Soc.*, 2020, **142**, 9567–9581.
11 J. He, N. J. J. Johnson, A. Huang and C. P. Berlinguette, *ChemSusChem*, 2018, **11**, 48–57.
12 J. Albero, Y. Peng and H. García, *ACS Catal.*, 2020, **10**, 5734–5749.
13 K. H. Ng, S. Y. Lai, C. K. Cheng, Y. W. Cheng and C. C. Chong, *Chem. Eng. J.*, 2021, **417**, 128847.
14 F. Puntoriero, G. La Ganga, A. M. Cancelliere and S. Campagna, *Curr. Opin. Green Sustainable Chem.*, 2022, **36**, 100636.
15 Y. Kuramochi and A. Satake, *Catalysts*, 2023, **13**, 282.
16 Y. Pellegrin and F. Odobel, *Comptes Rendus Chimie*, 2017, **20**, 283–295.
17 (*a*) A. Arrigo, F. Puntoriero, G. La Ganga, S. Campagna, M. Burian, S. Bernstorff and H. Amenitsch, *Chem*, 2017, **3**, 494–508; (*b*) F. Puntoriero, F. Nastasi, G. La Ganga, A. M. Cancelliere, G. Lazzaro and S. Campagna, *Multicomponent Supramolecular Photochemistry in Comprehensive Inorganic Chemistry III*, Elsevier, Third Edition, 2023, 628–653.
18 Y. Yamazaki, H. Takeda and O. Ishitani, *J. Photochem. Photobiol., C*, 2015, **25**, 106–137.
19 A. Arrigo, F. Nastasi, G. La Ganga, F. Puntoriero, G. Zappalà, A. Licciardello, M. Cavazzini, S. Quici and S. Campagna, *Chem. Phys. Lett.*, 2017, **683**, 96–104.
20 A. Arrigo, G. La Ganga, F. Nastasi, S. Serroni, A. Santoro, M.-P. Santoni, M. Galletta, S. Campagna and F. Puntoriero, *C. R. Chim.*, 2017, **20**, 209–220.
21 Y. Tamaki and O. Ishitani, *ACS Catal.*, 2017, **7**, 3394–3409.
22 (*a*) H. Ozawa and K. Sakai, *Chem. Commun.*, 2011, **47**, 2227–2242; (*b*) A. A. Ismail and D. W. Bahnemann, *Sol. Energy Mater. Sol. Cells*, 2014, **128**, 85–101; (*c*) K. Kitamoto and K. Sakai, *Chem. Commun.*, 2016, **52**, 1385–1388.
23 P. Zhou, I. A. Navid, Y. Ma, Y. Xiao, P. Wang, Z. Ye, B. Zhou, K. Sun and Z. Mi, *Nature*, 2023, **613**, 66–70.
24 S. Ye, C. Ding, M. Liu, A. Wang, Q. Huang and C. Li, *Adv. Mater.*, 2019, **31**, 1902069.
25 R. Matheu, P. Garrido-Barros, M. Gil-Sepulcre, M. Z. Ertem, X. Sala, C. Gimbert-Suriñach and A. Llobet, *Nat. Rev. Chem.*, 2019, **3**, 331–341.
26 B. Zhang and L. Sun, *J. Am. Chem. Soc.*, 2019, **141**, 5565–5580.
27 H. Zhang, W. Tian, X. Duan, H. Sun, S. Liu and S. Wang, *Adv. Mater.*, 2020, **32**, 1904037.
28 M. D. Kärkäs, O. Verho, E. V. Johnston and B. Åkermark, *Chem. Rev.*, 2014, **114**, 11863–12001.
29 N. Govindarajan and E. J. Meijer, *Inorganics*, 2019, **7**, 62.
30 P. Garrido-Barros, C. Gimbert-Suriñach, R. Matheu, X. Sala and A. Llobet, *Chem. Soc. Rev.*, 2017, **46**, 6088–6098.
31 M. Yagi and M. Kaneto, *Chem. Rev.*, 2001, **101**, 21–36.
32 L. Duan, A. Fischer, Y. Xu and L. Sun, *J. Am. Chem. Soc.*, 2009, **131**, 10397–10399.
33 S. W. Gersten, G. J. Samuels and T. J. Meyer, *J. Am. Chem. Soc.*, 1982, **104**, 4029–4030.
34 (*a*) C. Sens, I. Romero, M. Rodríguez, A. Llobet, T. Parella and J. Benet-Buchholz, *J. Am. Chem. Soc.*, 2004, **126**, 7798–7799; (*b*) R. Zong and R. P. Thummel, *J. Am. Chem. Soc.*, 2005, **127**, 12802–12803; (*c*) Z. Deng, H.-W. Tseng, R. Zong, D. Wang and R. Thummel, *Inorg. Chem.*, 2008, **47**, 1835–1848.
35 L. L. Zhang, Y. Gao, Z. Liu, X. Ding, Z. Yu and L. C. Sun, *Dalton Trans.*, 2016, **45**, 3814–3819.
36 T. Schlossarek, V. Stepanenko, F. Beuerle and F. Würthner, *Angew. Chem., Int. Ed.*, 2022, **61**, e202211445.
37 M. Schulze, V. Kunz, P. D. Frischmann and F. Würthner, *Nat. Chem.*, 2016, **8**, 576–583.
38 V. Kunz, M. Schulze, D. Schmidt and F. Würthner, *ACS Energy Lett.*, 2017, **2**, 288–293.
39 A.-L. Meza-Chincha, D. Schindler, M. Natali and F. Würthner, *ChemPhotoChem*, 2021, **5**, 173–183.
40 D. Schindler, A.-L. Meza-Chincha, M. Roth and F. Würthner, *Chem.–Eur. J.*, 2021, **27**, 16938–16946.
41 N. Noll and F. Würthner, *Chem.–Eur. J.*, 2021, **27**, 444–450.
42 M. Chen, S.-M. Ng, S.-M. Yiu, K.-C. Lau, R. J. Zeng and T.-C. Lau, *Chem. Commun.*, 2014, **50**, 14956–14959.
43 A. R. Howells, A. Sankarraj and C. Shannon, *J. Am. Chem. Soc.*, 2004, **126**, 12258–12259.
44 (*a*) A. Sartorel, M. Carraro, G. Scorrano, R. De Zorzi, S. Geremia, N. D. McDaniel, S. Bernhard and M. Bonchio, *J. Am. Chem. Soc.*, 2008, **130**, 5006–5007; (*b*) Y. V. Geletii, B. Botar, P. Koegerler, D. A. Hillesheim, D. G. Musaev and C. L. Hill, *Angew. Chem., Int. Ed.*, 2008, **47**, 3896; (*c*) N. D. McDaniel, M. J. Coughlin, L. L. Tinker and S. Bernhard, *J. Am. Chem. Soc.*, 2008, **130**, 210–217; (*d*) J. Limburg, J. S. Vrettos, L. M. Liable-Sands, A. L. Rheingold, R. H. Cabtree and G. W. Brudvig, *Science*, 1999, **238**, 1524–1527.
45 (*a*) V. Balzani, S. Campagna, G. Denti, A. Juris, S. Serroni and M. Venturi, *Acc. Chem. Res.*, 1998, **31**, 26–34; (*b*) S. Campagna, F. Puntoriero, F. Nastasi, G. Bergamini and V. Balzani, *Top. Curr. Chem.*, 2007, **280**, 117–214.
46 F. Puntoriero, G. La Ganga, A. Sartorel, M. Carraro, G. Scorrano, M. Bonchio and S. Campagna, *Chem. Commun.*, 2010, **46**, 4725–4727.
47 M. Bonchio, Z. Syrgiannis, M. Burian, N. Marino, E. Pizzolato, K. Dirian, F. Rigodanza, G. A. Volpato, G. La Ganga, N. Demitri, S. Berardi, H. Amenitsch, D. M. Guldi, S. Caramori, C. A. Bignozzi, A. Sartorel and M. Prato, *Nat. Chem.*, 2019, **11**, 146–153.
48 H. Lv, J. Song, Y. V. Geletii, J. W. Vickers, J. M. Sumliner, D. G. Musaev, P. Kögerler, P. F. Zhuk, J. Bacsa, G. Zhu and C. L. Hill, *J. Am. Chem. Soc.*, 2014, **136**, 9268–9271.
49 The authors consider the oxygen production in respect of the Ru^{3+} chemically producted.
50 M. Natali, I. Bazzan, S. Goberna-Ferrón, R. Al-Oweini, M. Ibrahim, B. S. Bassil, H. Dau, F. Scandola, J. R. Galán-Mascarós, U. Kortz, A. Sartorel, I. Zaharieva and M. Bonchio, *Green Chem.*, 2017, **19**, 2416–2426.
51 (*a*) T. J. R. Weakley, *J. Chem. Soc., Chem. Commun.*, 1984, 1406; (*b*) J. R. Galán-Mascarós, C. J. Gómez-Garcia, J. J. Borrás-Almenar and E. Coronado, *Adv. Mater.*, 1994, **6**, 221–223.

52 B. S. Bassil, S. Nellutla, U. Kortz, A. C. Stowe, J. van Tol, N. S. Dalal, B. Keita and L. Nadjo, *Inorg. Chem.*, 2005, **44**, 2659–2665.
53 M. Ibrahim, Y. Lan, B. S. Bassil, Y. Xiang, A. Suchopar, A. K. Powell and U. Kortz, *Angew. Chem., Int. Ed.*, 2011, **50**, 4708.
54 S. Tanakara, M. Annaka and K. Sakai, *Chem. Commun.*, 2012, **48**, 1653–1655.
55 N. Taira, K. Yamauchi and K. Sakai, *ACS Catal.*, 2023, **13**, 3211–3223.
56 L. Yu, Y. Ding and M. Zheng, *Appl. Catal., B*, 2017, **209**, 45–52.
57 M. Bösing, A. Nöh, I. Loose and B. Krebs, *J. Am. Chem. Soc.*, 1998, **120**, 7252–7259.
58 M.-P. Santoni, G. La Ganga, V. Mollica Nardo, M. Natali, F. Puntoriero, F. Scandola and S. Campagna, *J. Am. Chem. Soc.*, 2014, **136**, 8189–8192.
59 (*a*) C. Daniel and H. Hartl, *J. Am. Chem. Soc.*, 2005, **127**, 13978–13987; (*b*) C. Daniel and H. Hartl, *J. Am. Chem. Soc.*, 2009, **131**, 5101–5114.
60 J.-R. Shen, *Annu. Rev. Plant Biol.*, 2015, **66**, 23–48.
61 J. Lin, X. Liang, X. Cao, N. Weia and Y. Ding, *Chem. Commun.*, 2018, **54**, 12515.
62 X. Zhou, F. Li, H. Li, B. Zhang, F. Yu and L. Sun, *ChemSusChem*, 2014, **7**, 2453–2456.
63 A. Genoni, G. La Ganga, A. Volpe, F. Puntoriero, M. Di Valentin, M. Bonchio, M. Natali and A. Sartorel, *Faraday Discuss.*, 2015, **185**, 121–141.
64 J. K. Beattie, T. W. Hamblie, J. A. Klepetko, A. F. Masters and P. Turner, *Polyhedron*, 1998, **17**, 1343.
65 R. Chakrabarty, S. J. Bora and B. K. Das, *Inorg. Chem.*, 2007, **46**, 9450–9462.
66 O. Hodnebrog, M. Etminan, J. S. Fuglestvedt, G. Marston, G. Myhre, C. J. Nielsen, K. P. Shine and T. J. Wallington, *Rev. Geophys.*, 2013, **51**, 300–378.
67 T. R. Karl and K. E. Treberth, *Science*, 2003, **302**, 1719–1723.
68 H. Akimoto, *Science*, 2003, **302**, 1716–1719.
69 S. C. Roy, O. K. Varghese, M. Paulosea and C. A. Grimes, *ACS Nano*, 2010, **4**, 1259–1278.
70 Y. Kuramochi, O. Ishitani and H. Ishida, *Coord. Chem. Rev.*, 2018, **373**, 333–356.
71 D. Hildebrandt, D. Glasser, B. Hausberger, B. Patel and B. J. Glasser, *Science*, 2009, **323**, 1680–1681.
72 A. K. Singh, S. Singh and A. Kumar, *Catal. Sci. Technol.*, 2016, **6**, 12–40.
73 X. Yu and P. G. Pickup, *J. Power Sources*, 2008, **182**, 124–132.
74 J. Hawecker, J.-M. Lehn and R. Ziessel, *J. Chem. Soc., Chem. Commun.*, 1983, 536–538.
75 J. Hawecker, J.-M. Lehn and R. Ziessel, *Helv. Chim. Acta*, 1986, **69**, 1990–2012.
76 J.-M. Lehn and R. Ziessel, *Proc. Natl. Acad. Sci. U.S.A.*, 1982, **79**, 701–704.
77 Y. Yamazaki, H. Takeda and O. Ishitani, *J. Photochem. Photobiol., C*, 2015, **25**, 106–137.
78 S. Das and W. M. A. Wan Daud, *RSC Adv.*, 2014, **40**, 20856–20893.
79 Y. Tamaki, T. Morimoto, K. Koike and O. Ishitani, *Proc. Natl. Acad. Sci. U.S.A.*, 2012, **109**, 15673–15678.
80 (*a*) B. Gholamkhass, H. Mametsuka, K. Koike, T. Tanabe, M. Furue and O. Ishitani, *Inorg. Chem.*, 2005, **44**, 2326–2336; (*b*) Z.-Y. Bian, K. Sumi, M. Furue, S. Sato, K. Koike and O. Ishitani, *Dalton Trans.*, 2009, 983–993.
81 S. Meister, R. O. Reithmeier, A. Ogrodnik and B. Rieger, *ChemCatChem*, 2015, **7**, 3562–3569.
82 A. Umemoto, Y. Yamazaki, D. Saito, Y. Tamaki and O. Ishitani, *Bull. Chem. Soc. Jpn.*, 2020, **93**, 127–137.
83 A. M. Cancelliere, F. Puntoriero, S. Serroni, S. Campagna, Y. Tamaki, D. Saito and O. Ishitani, *Chem. Sci.*, 2020, **11**, 1556–1563.
84 A. Santoro, A. M. Cancelliere, K. Kamogawa, S. Serroni, F. Puntoriero, Y. T. S. Campagna and O. Ishitani, *Sci. Rep.*, 2023, **13**, 11320.
85 S. Shitaya, K. Nomura and A. Inagaki, *Chem. Commun.*, 2019, **55**, 5087–5090.
86 R. O. Reithmeier, S. Meister, B. Rieger, A. Siebel, M. Tschurl, U. Heiz and E. Herdtweck, *Dalton Trans.*, 2014, **43**, 13259–13269.
87 S. Sato, T. Morikawa, T. Kajino and O. Ishitani, *Angew. Chem., Int. Ed.*, 2013, **52**, 988–992.
88 R. O. Reithmeier, S. Meister, A. Siebel and B. Rieger, *Dalton Trans.*, 2015, **44**, 6466–6472.
89 T. Ouyang, H.-H. Huang, J.-W. Wang, D.-C. Zhong and T.-B. Lu, *Angew. Chem., Int. Ed.*, 2017, **56**, 738–743.
90 T. Ouyang, H.-J. Wang, H.-H. Huang, J.-W. Wang, S. Guo, W.-J. Liu, D.-C. Zhong and T.-B. Lu, *Angew. Chem., Int. Ed.*, 2018, **57**, 16480–16485.
91 S. Realista, J. C. Almeida, S. A. Milheiro, N. A. G. Bandeira, L. G. Alves, F. Madeira, M. José Calhorda and P. N. Martinho, *Chem.–Eur. J.*, 2019, **25**, 11670–11679.
92 J.-Q. Song, Y.-L. Lu, S.-Z. Yi, J.-H. Zhang, M. Pan and C.-Y. Su, *Inorg. Chem.*, 2023, **62**, 12565–12572.
93 J. Jökel, E. B. Boydas, J. Wellauer, O. S. Wenger, M. Robert, M. Römelt and U.-P. Apfel, *Chem. Sci.*, 2023, **14**, 12774–12783.
94 Z. Guo, G. Chen, C. Cometto, B. Ma, H. Zhao, T. Groizard, L. Chen, H. Fan, W.-L. Man, S.-M. Yiu, K.-C. Lau, T.-C. Lau and M. Robert, *Nat. Catal.*, 2019, **2**, 801–808.
95 (*a*) A. Paul, D. Connolly, M. Schulz, M. T. Pryce and J. G. Vos, *Inorg. Chem.*, 2012, **51**, 1977–1979; (*b*) Y. Kuramochi, M. Kamiya and H. Ishida, *Inorg. Chem.*, 2014, **53**, 3326–3332.
96 J. Bharti, L. Chen, Z. Guo, L. Cheng, J. Wellauer, O. S. Wenger, N. von Wolff, K.-C. Lau, T.-C. Lau, G. Chen and M. Robert, *J. Am. Chem. Soc.*, 2023, **145**(46), 25195–25202.
97 R. Giereth, M. Obermeier, L. Forschner, M. Karnahl, M. Schwalbe and S. Tschierlei, *ChemPhotoChem*, 2021, **5**, 644–653.
98 P. Lang, R. Giereth, S. Tschierlei and M. Schwalbe, *Chem. Commun.*, 2019, **55**, 600–603.
99 D. Hong, T. Kawanishi, Y. Tsukakoshi, H. Kotani, T. Ishizuka and T. Kojima, *J. Am. Chem. Soc.*, 2019, **141**, 20309–20317.

100 M. Sun, C. Wang, C.-Y. Sun, M. Zhang, X.-L. Wang and Z.-M. Su, *J. Catal.*, 2020, **385**, 70–75.
101 D. Liu, M. Zhang, H.-H. Huang, Q. Feng, C. Su, A. Mo, J.-W. Wang, Z. Qi, X. Zhang, L. Jiang and Z. Chen, *ACS Sustain. Chem. Eng.*, 2021, **9**, 9273–9281.
102 H. Yuan, J. Du, M. Ming, Y. Chen, L. Jiang and Z. Han, *J. Am. Chem. Soc.*, 2022, **144**, 4305–4309.
103 Y. Wang, L. Chen, T. Liu and D. Chao, *Dalton Trans.*, 2021, **50**, 6273–6280.
104 J.-R. Li, R. J. Kuppler and H.-C. Zhou, *Chem. Soc. Rev.*, 2009, **38**, 1477–1504.
105 (*a*) A. Dhakshinamoorthy, Z. Li and H. Garcia, *Chem. Soc. Rev.*, 2018, **47**, 8134–8172; (*b*) A. Dhakshinamoorthy, A. M. Asiri and H. Garcia, *Angew. Chem., Int. Ed. Engl.*, 2016, **55**, 5414–5445.
106 S. Qui and G. Zhu, *Coord. Chem. Rev.*, 2009, **253**, 2891–2911.
107 (*a*) S. Kandambeth, K. Dey and R. Banerjee, *J. Am. Chem. Soc.*, 2019, **141**, 1807–1822; (*b*) A. P. Cote, A. I. Benin, N. W. Ockwig, M. O'Keeffe, A. J. Matzger and O. M. Yaghi, *Science*, 2005, **310**, 1166–1170.
108 N. Huang, P. Wang and D. Jiang, *Nat. Rev. Mater.*, 2016, **1**, 16068.
109 (*a*) K. Guo, I. Hussain, G. Jie, Y. Fu, F. Zhang and W. Zhu, *J. Environ. Sci.*, 2023, **125**, 290–308; (*b*) Y. Zhang, H. Liu, F. Gao, X. Tan, Y. Cai, B. Hu, Q. Huang, M. Fang and X. Wang, *EnergyChem*, 2022, **4**, 100078; (*c*) Y. Yang, Y. Lu, H.-Y. Zhang, Y. Wang, H.-L. Tang, X.-J. Sun, G. Zhang and F.-M. Zhang, *ACS Sustain. Chem. Eng.*, 2021, **9**, 13376–13384; (*d*) Y.-H. Luo, L.-Z. Dong, J. Liu, S.-L. Li and Y.-Q. Lan, *Coord. Chem. Rev.*, 2019, **390**, 86–126; (*e*) J. Ozdemir, I. Mosleh, M. Abolhassani, L. F. Greenlee, R. R. Beitle Jr and M. H. Beyzavi, *Front. Energy Res.*, 2019, **7**, 77.
110 S. Navalòn, A. Dhakshinamoorthy, M. Álvaro, B. Ferrer and H. Garcìa, *Chem. Rev.*, 2023, **123**, 445–490.